Cosmic chemical evolution with an early population of intermediate-mass stars

Elisabeth Vangioni, Joseph Silk, Keith A. Olive, Brian D. Fields

Monthly Notices of the ROYAL ASTRONOMICAL SOCIETY

Mon. Not. R. Astron. Soc. **413,** 2987–3002 (2011) doi:10.1111/j.1365-2966.2011.18372.x

Cosmic chemical evolution with an early population of intermediate-mass stars

Elisabeth Vangioni,[1★] Joseph Silk,[2,3] Keith A. Olive[4] and Brian D. Fields[5]

[1]*Institut d'Astrophysique de Paris, UMR 7095 CNRS, University Pierre et Marie Curie, 98 bis Boulevard Arago, Paris 75014, France*
[2]*Department of Physics, University of Oxford, Keble Road, Oxford OX1 3RH*
[3]*Institut d'Astrophysique, UMR 7095 CNRS, University Pierre et Marie Curie, 98 bis Boulevard Arago, Paris 75014, France*
[4]*Theoretical Physics Institute, School of Physics and Astronomy, University of Minnesota, Minneapolis, MN 55455, USA*
[5]*Departments of Astronomy and of Physics, University of Illinois, Urbana, IL 61801, USA*

Accepted 2011 January 17. Received 2011 January 4; in original form 2010 November 4

ABSTRACT

We explore the effect of an early population of intermediate-mass stars in the 2–8 $M_\odot$ range on the cosmic chemical evolution. We discuss the implications of this population as it pertains to several cosmological and astrophysical observables. For example, some very metal poor Galactic stars show large enhancements of carbon, typical of the C-rich ejecta of intermediate-mass stars; moreover, halo star carbon and oxygen abundances show wide scatter, which imply a wide range of star formation and nucleosynthetic histories contributed to the first generations of stars. Also, recent analyses of the ^{4}He abundance in metal-poor extragalactic H II regions suggest an elevated abundance $Y_\mathrm{p} \simeq 0.256$ by mass, higher than the predicted result from the big bang nucleosynthesis, assuming the baryon density determined by the *WMAP*, $Y_\mathrm{p} = 0.249$. Although there are large uncertainties in the observational determination of ^{4}He, this offset may suggest a prompt initial enrichment of ^{4}He in early metal-poor structures. We also discuss the effect of intermediate-mass stars on the global cosmic evolution, the reionization of the Universe, the density of white dwarfs, as well as Type II supernovae (SN II) and SN Ia rates at high redshift. We also comment on the early astration of D and ^{7}Li. We conclude that if intermediate-mass stars are to be associated with Population III stars, their relevance is limited (primarily from observed abundance patterns) to low-mass structures involving a limited fraction of the total baryon content of the Universe.

Key words: stars: abundances – stars: Population II – stars: Population III – dark ages, reionization, first stars – large-scale structure of Universe.

1 INTRODUCTION

One of the outstanding questions concerning the first epoch of star formation is the stellar mass distribution of Population III stars. Most often, Population III stars are assumed to be very massive (40–100 $M_\odot$) or even more massive ($>100\,M_\odot$). Tracing chemical abundance patterns through the cosmic chemical evolution allows one to test theories employing massive Population III stars. For example, the abundance patterns seen in extremely iron poor stars do not support the hypothesis that the first stars had masses between 140–250 $M_\odot$ and end as pair-instability supernovae (PISNe, Daigne et al. 2004; Venkatesan et al. 2004). Note, however, that the apparent absence of any PISN signature in these halo stars could be due to an observational selection effect (Karlsson, Johnson & Bromm 2008), related to as yet unobserved elements which can be synthesized in PISNe, such as calcium. Yet other observations, such as those relating to the reionization history of the Universe, do point to an early population that is more massive than a standard Population I or II distribution. Here, we will explore the consequences of an early population of intermediate-mass (IM) (2–8 $M_\odot$) stars, which dominate at a redshift $z \sim 10$.

While there are many theoretical arguments pointing to very massive stars dominating Population III (Bromm & Larson 2004; Bromm et al. 2009), there exist arguments pointing to a first generation of stars with an initial mass function (IMF) peaked around the IM range. The current convention (Bromm et al. 2009) for terminology related to Population III stars is as follows: Population III.1 stars correspond to initial conditions determined only by cosmological parameters, while Population III.2 stars correspond to a second generation of stars with a lower typical mean mass which originate from the material polluted by Population III.1 stars. In this context, it is possible that the IM mode we discuss below is not so different from these Population III.2 stars. However, the typical Population III.2 mass is around 10 $M_\odot$ and includes Type II SNe (SNe II), while our mass range of 2–8 $M_\odot$ does not include any

★E-mail: vangioni@iap.fr

SNe and the correlated nucleosynthesis can be somewhat different. We also note that the metal-free IMF predicted from the opacity-limited fragmentation theory would peak around 4–10 $M_{\odot}$ with steep declines at both larger and smaller masses (Yoshii & Saio 1986). Primordial cosmic microwave background (CMB) regulated star formation also leads to the production of a population of early IM stars at low metallicity (Smith et al. 2009; Safranek-Shrader et al. 2010; Schneider & Omukai 2010).

On the observational side, there is abundant evidence for an early contribution from IM stars. IM stars have particular effects on chemical abundance patterns. Unlike their massive counterparts that end as core-collapse SNe, these stars produce very little in the way of heavy elements (oxygen and above), but produce significant amounts of carbon and/or nitrogen and above all helium. Indeed, there is evidence that the number of carbon enhanced stars increases at low iron abundances (Rossi, Beers & Sneden 1999), necessitating a Population III source of carbon, possibly in the asymptotic giant branch (AGB) phase of IM stars (Fujimoto, Ikeda & Iben 2000; Aoki et al. 2002; Lucatello et al. 2005). To account for the large [C,N/Fe] ratios found in a large number of extremely iron poor stars in our Galaxy, it was argued that an IMF peaked at 4–10 $M_{\odot}$ is needed (Abia et al. 2001). Furthermore, the presence of *s*-process elements, particularly Pb, at very low metallicity also points to AGB enrichment very early on (Aoki et al. 2001; Sivarani et al. 2004). As a result, an early population of IM stars may lead to a plausible explanation of recently observed carbon-enriched iron-poor stars. Note, however, that some SNe can also account for these high-carbon ejecta (Umeda & Nomoto 2005).

Isotopic abundances of C and Mg also lend clues to the early nucleosynthetic history of the Galaxy. Isotopic studies of the latter show a considerable amount of dispersion at low metallicity ranging from low values of ^{25,26}Mg/^{24}Mg, consistent with the pollution from core-collapse SNe, to high values of the Mg ratios, indicating the presence of the AGB production of the heavy Mg isotopes. Core-collapse SNe produce almost exclusively ^{24}Mg, while the observations of Yong, Lambert & Ivans (2003a) show enhancements (relative to predictions based on standard chemical evolution models) in both ^{25}Mg and ^{26}Mg. AGB stars were also concluded to be the source of the high ^{25,26}Mg/^{24}Mg ratios seen in the globular cluster NGC 6752 with [Fe/H] = −1.62 (Yong et al. 2003b). A similar conclusion was drawn in Alibés, Labay & Canal (2001) and Fenner et al. (2003).

Determining the identity and nature of the first stars is a primary goal in any attempt to understand the physics of the first billion years of the Universe. Cosmic chemical evolutionary models enable one to test many of the hypotheses for Population III stars (Ciardi & Ferrara 2005). The bulk of the existing work in this area considers either massive stars ($M > 40\ M_{\odot}$) or very massive stars ($M > 100\ M_{\odot}$). However, given the indications discussed above for an early population of IM stars, it seems crucial to examine the consequences for cosmic chemical evolution with IM Population III stars.

This paper is organized as follows. In Section 2, we discuss some of the expected consequences for a population of IM stars. These include (i) the effective prompt initial enrichment of helium, which we compare to recent determinations of primordial helium (Aver, Olive & Skillman 2010; Izotov & Thuan 2010) that show an excess relative to the predictions of the big bang nucleosynthesis (BBN); (ii) the reionization of the universe, usually ascribed to very massive Population III stars (Cen 2003; Haiman & Holder 2003; Wyithe & Loeb 2003; Bromm 2004); (iii) the evolution of the IMF; (iv) carbon-enhanced metal-poor stars; (v) the density of white dwarfs; (vi) the rate of SNe Ia at high redshift; and (vii) the evolution of N and Mg.

In Section 3, we introduce a relatively simple model of the galactic chemical evolution to highlight some of the (non-cosmological) effects of the IM stars, particularly on the evolution of element abundances based on the work of Fields et al. (2001). This model employs a bimodal star formation rate (SFR) which supplements a normal IMF and SFR, with one enhanced with IM stars. In Section 4, we introduce a cosmic chemical evolutionary model based heavily on the hierarchical models developed in Daigne et al. (2006) and Rollinde et al. (2009). We present our results in Section 5. Discussion and concluding remarks are given in Section 6.

2 CONSEQUENCES OF AN EARLY POPULATION OF INTERMEDIATE-MASS STARS

2.1 The primordial helium abundance

Among the successes of the *WMAP* determination of cosmological parameters is the accurate determination of the baryon density, $\Omega_B h^2$, or equivalently the baryon-to-photon ratio $\eta \equiv n_b/n_\gamma = 10^{-10}\eta_{10}$; Komatsu et al. (2009, 2011) find

$$\eta_{10} = 6.19 \pm 0.15. \quad (1)$$

As a consequence, it has become possible to treat the standard BBN as a zero-parameter theory (Cyburt, Fields & Olive 2002, 2003), resulting in relatively precise predictions of the light-element abundances of D, ^{3}He, ^{4}He and ^{7}Li (Cyburt, Fields & Olive 2001; Coc et al. 2002, 2004; Cuoco et al. 2004; Cyburt 2004; Descouvemont et al. 2004; Serpico et al. 2004; Cyburt, Fields & Olive 2008; Coc & Vangioni 2010).

When compared with current observational determinations of the abundances of D, ^{4}He and ^{7}Li, we find varying degrees of concordance, none of which is perfect. Deuterium is typically credited as being responsible for the concordance between the BBN and CMB determination of η. At the current value of η (equation 1), the deuterium abundance is predicted to be D/H = $(2.52 \pm 0.17) \times 10^{-5}$. This can be compared with the abundance of deuterium measured in quasar absorption systems. The weighted mean value of seven systems with reliable abundance determinations is D/H = $(2.82 \pm 0.21) \times 10^{-5}$ (Pettini et al. 2008, and references therein). However, the individual measurements of D/H show considerable scatter (a variance of 0.53) and it is likely that systematic errors dominate the uncertainties. While the agreement is certainly reasonable, we do draw attention to the fact that the predicted abundance is somewhat *lower* than the observed mean and this (slight) discrepancy will serve as a constraint below.

The discrepancy between the predicted abundance of ^{7}Li and the value found in halo dwarf stars is well documented (Cyburt et al. 2008). At the *WMAP* value of $\eta_{10} = 6.19$, ^{7}Li/H = $(5.12^{+0.71}_{-0.62}) \times 10^{-10}$, which is considerably higher than most observational determinations (Spite & Spite 1982; Spite et al. 1996; Ryan et al. 2000; Asplund et al. 2006; Bonifacio et al. 2007; Hosford et al. 2009, 2010). For example, the recent analysis of Sbordone et al. (2010) finds ^{7}Li/H = $(1.58 \pm 0.31) \times 10^{-10}$. We comment below on the possible effects of the astration in chemical evolution models on the lithium abundance.

Among the light elements, helium has the most accurately predicted primordial abundance. In addition, it is relatively insensitive to the baryon density and at $\eta = 6.19$, the helium mass fraction is

$$Y_p = 0.2487 \pm 0.0002. \quad (2)$$

The standard BBN results obtained in Coc & Vangioni (2010) are similar to those given above [$Y_p = 0.2475 \pm 0.0004$, D/H = $(2.68 \pm 0.15) \times 10^{-5}$, ^{7}Li/H = $(5.14 \pm 0.50) \times 10^{-10}$].

On the observational side, the determination of the helium abundance in extragalactic H II regions is fraught with difficulties (Olive & Skillman 2001). Over the last 15 yr, improvements in the analysis have led to a systematically higher ^{4}He abundance. Izotov, Thuan & Lipovetsky (1994) and Peimbert, Peimbert & Ruiz (2000) introduced a 'self-consistent' method for determining the abundance of ^{4}He simultaneously with the determination of the physical parameters associated with the H II region. They found $Y_p = 0.240 \pm 0.005$ and 0.235 ± 0.002, respectively. Using the Monte Carlo methods described in Olive & Skillman (2001) and selected high-quality data from Izotov et al. (1994), Olive & Skillman (2004) found a higher value with considerably larger uncertainties, $Y_p = 0.249 \pm 0.009$.

Further improvements to the analysis were aided by new atomic data (Porter, Ferland & MacAdam 2007) used in Peimbert, Luridiana & Peimbert (2007) and Izotov, Thuan & Stasinska (2007), where higher helium mass fractions were obtained, 0.2477 ± 0.0029 and 0.2516 ± 0.0011, respectively, based on the new He I emissivities and the collisional excitation of H I. The more recent work of Izotov & Thuan (2010) found a still higher value $Y_p = 0.2565 \pm 0.0010$ (statistical) ± 0.0050 (systematical). Using the same relatively small set of high-quality data from Izotov et al. (1994), Aver et al. (2010) found a similarly high value of $Y_p = 0.2561 \pm 0.0108$. The latter was a combined and uniform treatment of both hydrogen and helium emission lines, the inclusion of the new He emissivities, the effects of the underlying absorption, including their wavelength dependence, and neutral hydrogen collisional corrections. Strong degeneracies leading to large uncertainties in the individual helium abundance determinations were found in an unrestricted Monte Carlo analysis. These degeneracies and the limited range in O/H used in the regression to determine the primordial (O/H = 0) helium abundance combine to give the large uncertainty of 0.0108 and makes it certain that this determination is consistent with the BBN prediction at the *WMAP* value of η. Given the short baseline of this data set, it may be argued that a weighted mean of the helium results is warranted rather than the commonly used regression of Y versus O/H as in the case of all results quoted above. The weighted mean found in Aver et al. (2010) is

$$Y_p = 0.2566 \pm 0.0028 \qquad (3)$$

and one could be tempted to claim a slight discrepancy between the predicted and derived ^{4}He abundances.

If the central value of Y_p is indeed 0.256, rather than invoking the non-standard BBN or a non-standard cosmological history, it may be possible to argue for a prompt initial enrichment of He by an early population of stars. While the helium data responsible for Y_p are at relatively low metallicity, the most-metal-poor H II region used in the analysis leading to equation (3) is about 1/20 of the solar metallicity. There is therefore a reasonable possibility that some helium was produced early in the star formation history of pre-galactic structures. Here, we consider specific models of the chemical evolution which may be responsible for such a prompt initial enrichment of ^{4}He, remaining at the same time consistent with a multitude of evolutionary constraints.

2.2 Reionization

When the *WMAP* first reported their result for a large optical depth due to electron scattering (Kogut et al. 2003), which suggested a very early epoch of reionization of the intergalactic medium (IGM), it had an immediate impact on theories of the cosmic chemical evolution. The reported optical depth of $\tau_e = 0.17 \pm 0.04$ implied a redshift of reionization, $z_r \approx 20$. This put an immense amount of pressure on the models of the first stars and certainly pointed towards very massive stars as a potential solution (Cen 2003; Haiman & Holder 2003; Wyithe & Loeb 2003; Bromm 2004; Daigne et al. 2004). In subsequent analyses by the *WMAP* (Komatsu et al. 2011), the optical depth was lowered and currently it is reported to be $\tau_e = 0.088 \pm 0.015$, corresponding to $z_r = 10.5 \pm 1.2$. This change is significant as it greatly relaxes the constraints imposed on the models. First, the reionization at the relatively late redshift of 11 allows more time for structures and stars to form and more importantly at a later time, more baryons are incorporated in structures (in the hierarchical structure formation picture), and this decreases the ionizing flux per star needed for reionization.

The early epoch of reionization is one of the driving forces behind the identification of Population III stars with very massive stars. However, it has been argued that the number of very massive Population III stars needed for reionization would produce metal enrichments in conflict with observations (Daigne et al. 2004; Venkatesan et al. 2004). On the other hand, it has been shown that a 'normal' population of stars (i.e. a model with a standard SFR and Salpeter IMF) does not produce enough ionization photons so as to reionize the IGM (Daigne et al. 2004, 2006). Because of the short timescales involved (to achieve reionization by a redshift of 11), only stars with masses $M \gtrsim 3\,M_\odot$ can contribute to reionizing the IGM by a redshift of 11. There have been many studies that have shown that massive stars are fully capable of reionizing the IGM. For example, a bimodal model of star formation (with massive stars in the range 40–100 $M_\odot$) had been considered by Daigne et al. (2004, 2006). Detailed studies (Johnson et al. 2009; Wise & Cen 2009; Robertson et al. 2010) have modelled the reionization in a more realistic way. Indeed, in the past, there was probably a complicated mix of stellar IMF and SFR modes at high redshift. In this context, the escape fraction which is determined by complex radiation hydrodynamics is expected to increase with redshift; the photoheating process depends on the presence of massive stars which are clearly required for high-redshift reionization. Nevertheless, to the best of our knowledge, the capabilities of IM stars have yet to be explored in this context. Although our main aim in this paper is to study the nucleosynthetic aspects of IM stars, we will show below that these stars are capable of reionizing the IGM sufficiently rapidly at redshift about 10, though that does not exclude the role of more massive stars at higher redshift.

2.3 Evolution of the IMF

One can make a phenomenological case from galaxy evolution for an IM-star-dominated IMF at $z \gtrsim 2$. The arguments are individually refutable but the cumulative effect is certainly suggestive.

(i) Comparison of the cosmic SFR with the rate of change in the local stellar mass density reveals a discrepancy at $z \gtrsim 2$ that increases towards higher z. Integration of the cosmic SFR yields a larger stellar mass density than observed. The discrepancy is such that one *apparently* requires a reduced ratio of the stellar mass to luminosity in star-forming galaxies. This is achievable if the IMF has an excess of IM stars at these epochs. No universal power-law fit is acceptable at $z \gtrsim 0.5$ according to Wilkins et al. (2008a). A similar discussion also leads to a preferred SFR at $z \gtrsim 3$ that is approximately three times higher than the best fit to the stellar mass density (Wilkins, Trentham & Hopkins 2008b). There are other possible explanations, including uncertainties in stellar mass measurements and dust extinction, but none of these is preferred.

(ii) Comparison of the rate of the luminosity evolution of massive early-type galaxies in clusters at $0.02 < z < 0.83$ to the rate of their colour evolution requires that the IMF is weighted towards more massive stars at earlier epochs. A specific interpretation is that the characteristic stellar mass ($\sim$0.3 $M_{\odot}$ today) had a value of $\sim$2 $M_{\odot}$ at $z \sim 4$ (van Dokkum 2008).

(iii) The evolution of the galaxy stellar mass–SFR relationship for star-forming galaxies constrains the stellar mass assembly histories of galaxies. Simulations including gas accretion reproduce a tight correlation but the evolution with redshift disagrees with the data. The simulations generally prefer a constant specific SFR $\dot{M}_*/M_*$. The specific SFR is high at $z \gtrsim 2$, remains high to $z \sim 7$, but is low today (Gonzalez et al. 2010a). To reconcile these results with the simulations, Davé (2008) proposed that the stellar IMF evolves towards more high-mass star formation at earlier epochs such that the characteristic stellar mass in the IMF varies approximately from the present as $(1 + z)^2$ to $z \sim 2$.

The arguments listed above apply to the high-redshift universe where the dominant contributors to both the light and the stellar mass are massive starbursting galaxies. There is also some intriguing evidence from the local Universe that differentiates the IMF in current-epoch luminous star-forming galaxies from their lower luminosity counterparts.

Nearby massive star-forming galaxies seem to have an IMF that is more massive star dominated than lower mass galaxies. There is evidence for a non-universal stellar IMF from the integrated properties of SDSS galaxies, according to Hoversten & Glazebrook (2008). These authors inferred the stellar IMF from the integrated light properties of galaxies by comparing galaxy Hα equivalent widths (EWs) with a broad-band colour index to constrain the IMF. They find that low-luminosity galaxies have much lower EW(H I) than expected for their colours and argue that this is due to the IMF in low-luminosity galaxies having fewer massive stars, either by a steeper slope or by a lower upper-mass cut-off, than that for luminous galaxies.

A similar result for H I-selected galaxies emerges via the Hα and the far-ultraviolet (FUV) continuum tracers of star formation. Meurer et al. (2009) find that the flux ratio, Hα/FUV, shows strong correlations with the surface brightness in Hα and the *R* band: low surface brightness galaxies have lower ratios compared to high surface brightness galaxies. The most plausible explanation for the correlations are systematic variations in the upper mass limit and/or slope of the IMF at the upper end. Massive galaxies in the local universe have an IMF that is preferentially enhanced in massive stars relative to low-mass galaxies.

It seems that a case can be made that galaxies which form stars rapidly, specifically massive galaxies at high redshift and their nearby counterparts, possess an IMF that is relatively top-heavy (or bottom-light). We can speculate that essentially all vigorously star-forming systems at high redshift may similarly possess an IMF enriched in IM stars. These at least are the building blocks that in our model provide the sources of the bulk of ionizing photons at z as high as $\sim$10 and play a role in the recycling of processed gas.

2.4 Carbon-enhanced metal-poor stars, carbon-rich ultra-metal-poor stars and the transition discriminant $D_{\rm trans}$

It is well known that massive Population III stars have a very specific impact on the nucleosynthesis budget of the early Universe. In this context, it is useful to incorporate stellar halo observations, specifically from extremely metal poor stars ([Fe/H] < -3), ultra metal poor stars ([Fe/H] < -4) and hyper metal poor stars ([Fe/H] < -5) to derive constraints on the mass range of massive Population III stars. From the nucleosynthetic point of view, halo stars have long been used to constrain galactic chemical evolution models, but were, until recently, quite disconnected from cosmological models. Indeed, these old low-mass stars preserve their pristine composition on their surface. The abundance patterns seen in these metal-poor stars, originating presumably from Population III stars, can yield very precious information about the first nucleosynthesis processes in the Universe (subsequent to the big bang) and thus gives one the possibility of exploring the Universe during the period of reionization (Frebel, Johnson & Bromm 2007; Frebel 2010).

Stellar models based on Woosley & Weaver (1995) used below do not take into account the effects of the rotation in stars (and specifically in primordial stars). Rotation has been shown to play an important role at zero and very low metallicity. Ekström et al. (2008) have demonstrated that nitrogen is boosted by the rotation and more generally the rotating models produce more metals than their non-rotating counterparts. Consequently, these rotating stars could leave a specific nucleosynthetic imprint on their surroundings which can have important consequences on the abundances in very low metallicity stars and the pollution of the IGM. Moreover, the rotation rate has important implications for the global evolution of primordial stars (see Stacy, Bromm & Loeb 2011).

On the other hand, it has been shown (Bromm & Loeb 2003; Frebel et al. 2007) that the abundances of ionized carbon and neutral atomic oxygen are important for the transition from the Population III to Population II/I star formation. Bromm & Loeb (2003) defined a transition discriminant

$$D_{\rm trans} = \log(10^{[{\rm C/H}]} + 0.3 \times 10^{[{\rm O/H}]}), \tag{4}$$

which clearly reveals the nucleosynthetic imprint of Population III stars. This function has the great advantage of being able to connect aspects of the cosmological evolution with the C/O abundances in low-mass stars. In this context, carbon-enhanced metal-poor stars or carbon-rich ultra-metal-poor stars (CEMPSs and CRUMPSs) seem to indicate an overabundance of carbon (and oxygen) at early stages of evolution. CEMPSs represent about 20 per cent of the metal-poor stars. Recent studies considering multizone chemical evolution models show that only models with increased C yields or an initial top-heavy IMF in the IM star mass range provide good fits of observations in the Milky Way (Mattsson 2010). Note that these models also predict a nitrogen enhancement which will be considered below. Therefore, from the nucleosynthesis viewpoint, it is interesting to consider IM stars as Population III candidates, since they are producers of both C and He.

Finally, observations of metal absorption features in the IGM give important constraints on models of the formation and evolution of the earliest structures. Recent measurements of C in the IGM (Cooke et al. 2010; Hultman Kramer, Haiman & Madau 2010) show an increase in this element at about $z = 6$. This seems to clearly indicate that an increase in the SFR at this redshift is able to produce carbon. Again, IM stars are good candidates for explaining this trend. Note that we also predict that IGM material could have a high C/O ratio; indeed, we can obtain insight into this ratio from observations, though presently, it is difficult to obtain reliable C/O ratios from ionized abundance data (namely C IV and O VI).

2.5 Element abundances: N and Mg

In the course of the standard stellar evolution, nitrogen is produced through He burning. Primary nitrogen is also synthesized in massive stars in the H burning layer via fresh carbon coming from the He burning core. In IM stars, nitrogen is produced together with carbon. Hot bottom-burning plays a dominant role for the synthesis of N and the amount of nitrogen produced depends on the efficiency and the duration of nuclear burning. At lower metallicity, the production of nitrogen is favoured over carbon. There are indeed systems at low metallicity, such as 47 Tuc and M71, which show large nitrogen enhancements (Harbeck, Smith & Grebel 2003; Briley et al. 2004). Abundance patterns found in these systems make it difficult to argue that the nitrogen enhancements are due to the internal contamination and lend credence to the hypothesis of an early IM stellar population (Ashenfelter, Mathews & Olive 2004).

The evolution of the nitrogen abundance is very sensitive to specific parameter choices in the chemical evolution model (Ashenfelter et al. 2004). Included among these are the uncertainties stemming from the yields (Karakas & Latanzzio 2007) particularly in the upper end of the IM range (>3 $M_\odot$). Unfortunately, this element is difficult to observe. Indeed, the best measurements come from the CN BX electronic transition band which is not generally detected. In this context, it is difficult to confront the calculated evolution of this element with available observations. However, it is interesting to note that N is observed in a few CEMPSs as shown below. Magnesium is produced predominantly in SNe II where it is formed in the carbon- and neon-burning shells in massive stars. The dominant isotope formed in SNe II is ^{24}Mg. The neutron-rich isotopes, ^{25}Mg and ^{26}Mg, are produced in the outer carbon layer through α capture on neon. The yield of the heavier isotopes scales with the metallicity in the carbon layer and as a result very little of these isotopes are produced at low metallicity. In contrast, significant amounts of ^{25}Mg and ^{26}Mg are produced during the hot bottom-burning in the AGB phase in IM stars (Boothroyd, Sackmann & Wasserburg 1995). These stars are hot enough for efficient proton-capture processes on Mg leading to Al (which decays to the heavier Mg isotopes). The neutron-rich isotopes are also produced during thermal pulses of the helium-burning shell. Here, α capture on ^{22}Ne (which is produced from α capture on ^{14}N) leads to both ^{25}Mg and ^{26}Mg. The latter process is very important for ≈ 3 $M_\odot$ (Karakas & Latanzzio 2003). Several observations (Shetrone 1996; Yong et al. 2003a,b) indicate enhancements of the neutron-rich isotopes in low-metallicity stars which could necessitate the presence of an early population of IM stars (Alibés et al. 2001; Fenner et al. 2003; Ashenfelter et al. 2004).

Finally, it is interesting to note that Mg has been observed in ultrafaint dwarf galaxies (Frebel & Bromm 2010) which are representative of the nucleosynthetic processes in the first galaxies. Specifically, in spite of the uncertainties related to the Mg data in these objects, we also note that the [Mg/Fe] ratio is somewhat higher (about 1) in these structures compared to the local data (about 0.3) in fig. 1 of Frebel & Bromm (2010). Once again this could be a signature of the presence of IM stars in these primitive galaxies.

2.6 White dwarfs

The best current limits on the halo old white dwarf population come from a combination of interpreting the MACHO and EROS microlensing events with an improved white dwarf atmosphere modelling (Torres et al. 2010). The upper limit, including white dwarfs with hydrogen-deficient atmospheres, allows an increased microlensing optical depth. The upper limit to the contribution of halo white dwarfs is comparable to that of the thick disc and accounts for at most 10 per cent of the halo dark matter between the Milky Way Galaxy (MWG) and the Large Magellanic Cloud. The MACHO upper limit reported in Alcock et al. (2000) is around 40 per cent with a possible detection at 20 per cent (central value). The EROS subsequently discovered that one of the MACHO candidates was a variable star and Bennett (2005) reduced the favoured MACHO value to 16 per cent. The EROS independently presented an upper limit of 8 per cent (Tisserand et al. 2007). For comparison, our IM Population III component gives a white dwarf mass fraction very comparable to the standard one; it differs only by 15 per cent (see Fig. 3 shown later). Note that Chabrier (2004) had already examined the possibility that a part of the baryon content at high redshift could be trapped in a white dwarf remnant population coming from an early population of IM stars. He concluded that this background contribution could increase appreciably with redshift.

2.7 SN rates

Among the important constraints imposed on the models of the cosmic chemical evolution are the rates of SNe. These are intimately linked to the choice of an IMF and SFR, and represent an independent probe of the star-forming universe. While Type II rates directly trace the star formation history, there is a model-dependent time-delay between the formation (and lifetime) of the progenitor star and the SN Ia explosion. Since existing data are available only for relatively low redshifts, we discuss the predicted SN rates in the context of three different models and give some constraints related to the SNe Ia rate coming from the IM star mode.

Our early IM stellar population hypothesis inevitably produces many SNe at high redshift. The predicted SFR and SN rates are presented below. The SFR rate corrections (for dust, luminosity function, etc.) are notoriously unreliable at $z \gtrsim 8$ where our IM population (predominantly formed earlier than $z \sim 10$) makes a significant contribution. The SN Ia rates provide a potentially more robust discriminant. However, we note here that three issues help reconcile our SN rate predictions with observations of SNe Ia at $z \gtrsim 1$. Most importantly, the selection efficiency of SNe Ia, in the absence of near-infrared selection, dives rapidly to zero at high redshift (beyond $z \sim 1.5$). Indeed, from Perrett et al. (2010), the extrapolation of the efficiency to $z = 2$ implies a steep drop (to only a fraction of a per cent). Moreover, the SN Ia precursors are predominantly in low-mass galaxies, which contain subluminous SNe Ia, by as much as 0.5 mag (Sullivan et al. 2010). Thirdly, it may be that at low metallicity ([Fe/H] < -1.1), the absence of iron lines driving optically thick winds may greatly inhibit the number of SNe Ia (Nomoto et al. 2003). Finally, note that there are large uncertainties related to the time-delay between IM-star formation and the resulting SN Ia explosion. These uncertainties add to the complexity of the question, since the predicted bulk of SNe Ia can be found at higher or lower high redshift, according to the value of this time-delay (Totani et al. 2008).

3 STANDARD CHEMICAL EVOLUTION MODEL

There are only a few basic ingredients to a standard (non-cosmological) galactic evolution model. These include the specification of an IMF, usually assumed to be a power law of the form $\phi(m) \sim m^{-x}$; a SFR, which may be proportional to some power of the gas mass fraction or a specified function of time; and a specification of stellar properties such as lifetimes and elemental yields. More complex models will include the infall of gas from the IGM and outflows from stellar-induced winds. Certain observations such as the metallicity distribution in low-mass stars may call for the prompt initial enrichment of metals which can be accomplished using bimodal models of the chemical evolution in which a standard mode (e.g. a Salpeter IMF and a SFR proportional to the gas fraction) is supplemented with a shallow IMF providing predominantly massive stars over a brief period of time (or metallicity). In this section, we will show that this approach cannot work for the prompt enrichment of ^{4}He as the most-massive stars would produce heavy elements very early and thus would not enhance the ratio of He to metals. In other words, the enrichment of He would occur too late and would not explain the enhancement in low-metallicity regions.

In contrast, bimodal models which are augmented with a population of IM stars (with the mass between 2–8 $M_\odot$) can indeed provide an enrichment of He at low metallicity in simple galactic chemical evolution models. While the model presented in this section cannot directly be extended to a model of the cosmic chemical evolution, it does provide some insight into the needed bimodality involving IM stars that will carry over into a more sophisticated model based on the hierarchical structure formation as in Daigne et al. (2006).

In Fields et al. (2001), we constructed chemical evolution models which led to significant D astration at low metallicity and also had significant white dwarf production. These models were based on a bimodal construction where the 'massive' mode consisted of IM stars. Here we consider the effect of such models on the ^{4}He production at low metallicity.

We illustrate results with the simple closed-box model of Fields et al. (2001), which neglects both the infall and outflow of baryons. The baryonic cycling through stars is determined by the creation function $C(m, t)$:

$$dN_\star = C(m, t)\, dm\, dt, \tag{5}$$

which describes the mass distribution of new stars and the total SFR $\Psi(t) = \int C(m, t) dm$. We adopt a 'bimodal' creation function

$$C(m, t) = \psi_1(t)\phi_1(m) + \psi_2(t)\phi_2(m), \tag{6}$$

each term of which represents a distinct star formation mode.

In the first term of equation (6), we encode an early burst of IM star formation; to do this, we adopt the SFR

$$\psi_1 = x_{\rm burst} \frac{M_{\rm B}}{\tau_1} e^{-t/\tau_1}, \tag{7}$$

with a burst time-scale $\tau_1 = 100$ Myr. The parameter $x_{\rm burst}$ controls the fraction of the baryonic mass $M_{\rm b}$ which is processed in the burst; we will show results for different values of this parameter, but clearly we must have $x_{\rm burst} \le 1$. Since our focus is on IM stars, the IMF for this mode is a power-law (Salpeter) form: $\phi(m) \propto m^{-2.3}$, for $m \in [2\,M_\odot, 8\,M_\odot]$.

The second term in equation (6) describes normal star formation. Again, following Fields et al. (2001), we adopt the classic form $\psi_2 = \lambda g(t) M_{\rm gas}$, with $\lambda = 0.3\,{\rm Gyr}^{-1}$ and a smoothing factor $g(t) = 1 - e^{-t/0.5\,{\rm Gyr}}$, which ensures that the star formation begins in the bursting IM mode, which then smoothly goes over to the standard mode. The normal-mode IMF is of the Salpeter form $\phi_2(m) \propto m^{-2.6}$, but now with $m \in [0.1\,M_\odot, 100\,M_\odot]$. Both IMFs are normalized in the usual way $\int m\,\phi_2(m)\,dm = 1$.

In Fig. 1, we show the evolution of the ^{4}He mass fraction, Y, as a function of the oxygen abundance (relative to solar oxygen).

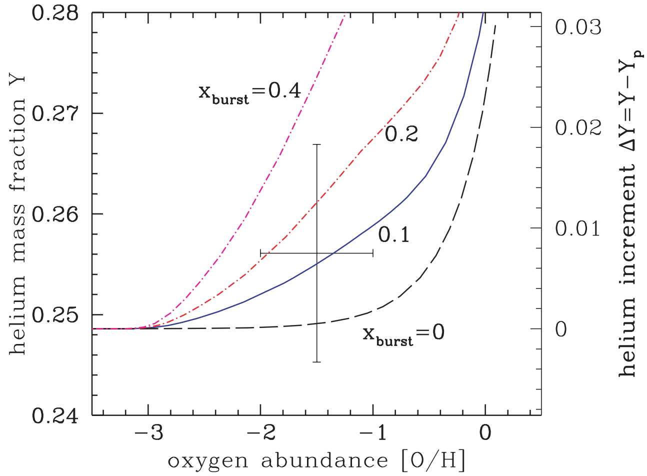

Figure 1. The ^{4}He mass fraction in several bimodal models of chemical evolution. Curves show different fractions $x_{\rm burst}$ (equation 7) of baryons processed through the burst phase. The data point is representative of the helium data in low-metallicity extragalactic H II regions.

Curves are shown for different values of the burst mass fraction $x_{\rm burst}$ in equation (7). In the case of normal star formation (i.e. when $x_{\rm burst} = 0$ and the IM mode is absent), as O increases, we see He rise from its primordial value, but undershoots the low-metallicity data. That normal star formation fails to match the data traces back to nucleosynthesis patterns in high-mass stars, which dominate the production of O and of new He in this scenario. Specifically, for high-mass stars, the ejecta have $\Delta Y/\Delta Z_{\rm O} \sim 1$, that is, comparable masses of new He and of O (Woosley & Weaver 1995). Thus, at low metallicity $Z_{\rm O} \ll Z_{{\rm O},\odot} \sim 0.01$, we have $\Delta Y \ll 0.01$, whereas the data seem to require $\Delta Y_{\rm obs} \simeq 0.01$. This not only explains the problem with this simple scenario, but also suggests the solution: invoke a stellar population which has substantially different helium and metal nucleosynthesis.

Indeed, Fig. 1 shows that as we turn to the bursting IM mode via $x_{\rm burst} > 0$, there is an abrupt rise in He at low O abundances, with a larger rise for larger $x_{\rm burst}$. As anticipated, this rise now allows for the predictions to match the data, with good fits for $x_{\rm burst} \sim$ 10–20 per cent. The origin of this rise clearly reflects the nucleosynthesis patterns of IM stars, whose ejecta are much more enriched in new He than in O, relative to massive stars. Specifically, for IM stars at low metallicity in the $m = (4\,M_\odot, 8\,M_\odot)$ we have $\Delta Y/\Delta Z_{\rm O} \sim (50, 300)$ (van den Hoek & Groenewegen 1997). These large ratios trace back to the very small O production in these stars.

The results thus far are for the simplest possible model: a single-zone closed box. Staying with single-zone models, even if we include infall and/or outflow, the results should be similar. In the case of primordial infall, both the metal and new He yields will be diluted, and by the same factor. Thus, the He–O trends should stay the same. Similarly, in the case of outflows, the abundances in the gas remaining in the box are only affected if the flow ejects one element preferentially relative to the other. But again, given that O and new He are produced in the same environments, any physically realizable winds will remove them together, leaving the remaining gas with He–O trends unaffected.

The lessons we draw from our simple model are that an increase in helium at low metallicity, as suggested by observations, can be accomplished at the cost of processing 10–20 per cent of observable cosmic baryons through IM stars. But as shown in Fields et al. (2001) and discussed above, such a scenario also has substantial consequences, including other element abundances, white dwarfs and SNe Ia. To examine all of these issues in a more realistic manner requires a chemical evolution model in a cosmological context.

4 A COSMOLOGICAL CHEMICAL EVOLUTION MODEL

4.1 Generalities

The study of the star formation in a cosmological context requires the inclusion of (i) a model of the dark matter structure formation; and (ii) accretion and outflow of the baryonic matter with respect to existing and forming structures.

We have developed a detailed model of the cosmological chemical evolution (Daigne et al. 2006; Rollinde et al. 2009) using a description of non-linear structures, based on the standard Press–Schechter (PS) formalism (Press & Schechter 1974). Baryons are placed (1) within stars or their remnants within collapsed structures; or (2) in gas within collapsed structures [the interstellar medium (ISM)]; or (3) outside of structures (IGM). The rate at which structures accrete mass is determined by a PS distribution function, $f_{\rm PS}(M, z)$. The model included the mass (baryon) exchange between the IGM and ISM, and between the ISM and stellar component. In this study, we assume that the minimum mass of dark matter haloes for star-forming structures is 10^7 M$_\odot$. This minimum mass was found to best fit observational constraints as a whole in a more complete study of the dependence of the dark matter halo mass (Daigne et al. 2006).

Once the model is specified, we can follow many astrophysical quantities, such as the global SFR, the optical depth, the SN rates and the abundances of individual elements (Y, D, Li, Fe, C, N, O and Mg abundances) which are used to tackle specific questions related to early star formation and the reionization epoch. In this study, we consider two distinct modes of star formation: a normal mode of Population II/I stars and a massive or IM mode of Population III stars.

Throughout this paper, a primordial power spectrum with a power-law index $n = 1$ is assumed and we adopt the cosmological parameters of the so-called concordance model (Komatsu et al. 2011), that is, $\Omega_{\rm m} = 0.27$, $\Omega_\Lambda = 0.73$, $h = 0.71$ and $\sigma_8 = 0.9$.

4.2 SFR scenarios

As in the simple model described in Section 3, the models considered are bimodal. Each model contains a normal mode with stellar masses between 0.1 and 100 M$_\odot$, with a near Salpeter IMF ($x = 1.6$) (hereinafter called model 2).

We fit the SFR history of Population II/I stars to the data compiled in Hopkins & Beacom (2006) (from $z = 0$ to 5) and to the recent measurements at high redshift by Bouwens et al. (2010) and Gonzalez et al. (2010b). These observations place strong constraints on the Population II/I SFR. The fit for the SFR, $\psi(z)$, is based on the mathematical form proposed in Springel & Hernquist (2003):

$$\psi(z) = \nu \frac{a \exp[b\,(z - z_{\rm m})]}{a - b + b \exp[a\,(z - z_{\rm m})]} \,. \quad (8)$$

The amplitude (astration rate) and the redshift of the SFR maximum are given by ν and $z_{\rm m}$, respectively, while b and $b - a$ are related to its slope at low and high redshifts, respectively. The normal mode is fitted using $\nu_{\rm II/I} = 0.3\,{\rm M_\odot\,yr^{-1}\,Mpc^{-3}}$, $z_{\rm m\,II/I} = 2.6$, $a_{\rm II/I} = 1.9$ and $b_{\rm II/I} = 1.1$. The SFR of this mode peaks at $z \approx 3$.

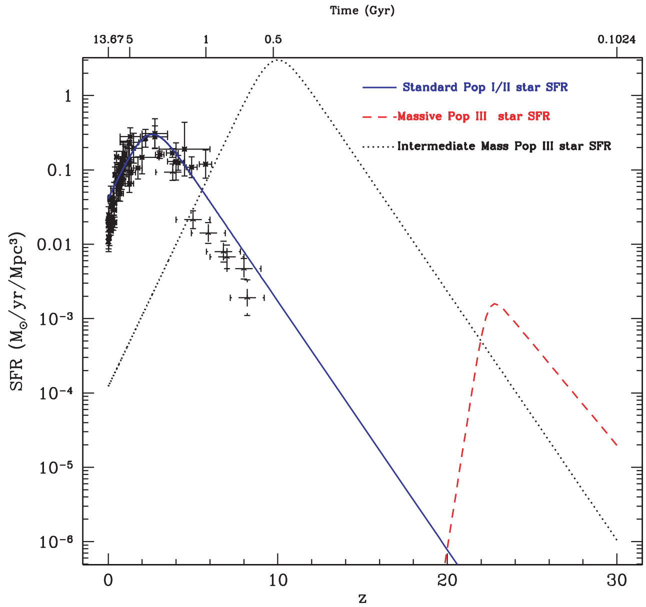

Figure 2. The cosmic SFR as a function of the redshift. The data (solid black points) are taken from Hopkins & Beacom (2006). The dashed black points come from Bouwens et al. (2010) and from Gonzalez et al. (2010b). The blue solid line represents the standard SFR with a Salpeter IMF and a mass range $0.1 < M/{\rm M_\odot} < 100$. The dashed red line represents the massive Population III stellar mode, with a Salpeter IMF and a mass range $36 < M/{\rm M_\odot} < 100$. The dotted black curve represents the IM SFR mode, with a Salpeter IMF and a mass range $2 < M/{\rm M_\odot} < 8$.

In addition to the normal mode, we add a mode for Population III stars. Our primary interest here is a model for IM Population III stars and we choose an IM component of stars with 2–8 M$_\odot$ (hereinafter model 3), assuming an IMF with slope 1.3. Some fraction of the IM stars become SNe Ia. The SFR parameters are the following: $\nu_{\rm IIIa} = 3\,{\rm M_\odot\,yr^{-1}\,Mpc^{-3}}$, $z_{\rm m\,IIIa} = 10$, $a_{\rm IIIa} = 1.9$ and $b_{\rm IIIa} = 1.1$. The redshift peak is chosen so that the IM stars are born in time to affect low-metallicity abundances and the normalization is chosen to allow a substantial effect on ^{4}He.

For comparative purposes, we also consider a massive component with stars between 36–100 M$_\odot$ with an IMF slope of 1.6, which terminate as SNe II (hereinafter model 1). The SFR parameters are the following: $\nu_{\rm IIIb} = 0.0016\,{\rm M_\odot\,yr^{-1}\,Mpc^{-3}}$, $z_{\rm m\,IIIb} = 22.8$, $a_{\rm IIIb} = 4$ and $b_{\rm IIIb} = 3.3$. For a detailed description of the model, see Rollinde et al. (2009) and Daigne et al. (2006). Note that both models 1 (massive) and 3 (IM) include the normal mode (model 2).

In Fig. 2, we show the adopted SFR for each of the three cases considered. As one can see, the normal mode is chosen to fit the observations also plotted in the figure. As the data extend only up to $z \approx 8$, there is essentially no constraint on the massive mode which dominates at $z \gtrsim 20$. Data at $z \gtrsim 8$ are highly uncertain due to unknown systematics involving, among other effects, the dust corrections and adopted rest-frame UV luminosity function, and present essentially no conflict with our models (Labbe, Gonzalez & Bouwens 2010).

Fig. 2 also shows that the IM mode represents a significant processing of baryons. The peak of the IM SFR is about a factor of ~10 higher than the peak of the normal SFR and a factor of ~10^3 higher than the massive Population III SFR. On the other hand, the IM star formation peak lasts for about a factor of ~10 less time than the normal SFR. Thus, we expect that roughly comparable amounts of baryons will be processed through these two modes. In contrast,

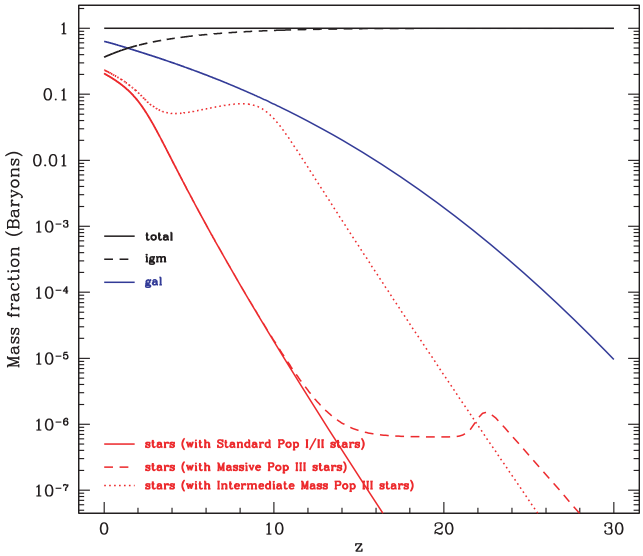

Figure 3. Different mass fractions as a function of the redshift. The flat solid black line (top of the figure) represents the total baryons in the Universe. The IGM fraction is shown by the dashed black curve and the galactic fraction is shown by the growing solid blue curve. The mass fraction of stars is plotted for the three models considered (red curves): solid line for model 2 (normal mode), dashed line for model 1 (with massive Population III stars) and the dotted line for model 3 (with IM stars).

a much smaller fraction of baryons are processed through the massive Population III mode. One should recall, however, that in our model many baryons always remain in the IGM and never reside in galaxies nor are processed through stars.

Fig. 3 represents the mass fraction of each component related to the total mass of baryons: IGM, galaxies and stars. Note that the addition of the IM star component does not affect the mass fraction of stars (including remnants) at low redshift.

Note that the star fraction in the IM mode has an initial peak at about ∼10 per cent of all baryons. This occurs at $z \sim 10$. The star fraction then drops as the IM stars die off, then rises with the normal star formation. Thus, we see that in our model, about 10 per cent of the baryons are processed through the IM mode. In contrast, we see that the massive Population III mode only processes about $\sim 10^{-6}$ of all baryons.

4.3 Yields and lifetimes

The lifetimes of IM stars ($0.9 < M/\mathrm{M}_{\odot} < 8$) are taken from Maeder & Meynet (1989) and from Schaerer (2002) for more massive stars. Old halo stars with masses below $\sim 0.9\,\mathrm{M}_{\odot}$ have a lifetime long enough to be observed today. They are assumed to inherit the abundances of the ISM at the time of their formation. Thus, their observed abundances reflect, in a complex way (due to exchanges with the IGM), the yields of all massive stars that have exploded earlier.

The yields of stars depend on their mass and metallicity, but not on their status (i.e. Population II/I or Population III). Some Population II/I stars are massive, although in only a very small proportion since we use a slightly steeper than the Salpeter IMF. Population III stars are all massive stars. We use the tables of yields (and remnant types) given in van den Hoek & Groenewegen (1997) for IM stars ($<8\,\mathrm{M}_{\odot}$) and the tables in Woosley & Weaver (1995) for massive stars ($8 < M/\mathrm{M}_{\odot} < 40$). An interpolation is made between different metallicities ($Z = 0$ and $Z = 10^{-4}, 10^{-3}, 10^{-2}, 10^{-1}$ and $10^{0}\,\mathrm{Z}_{\odot}$) and we extrapolate the tabulated values beyond $40\,\mathrm{M}_{\odot}$.

5 RESULTS

Having specified the models under consideration, we can now systematically consider the consequences of our particular choices for Population III stars. For most of the results which follow, we will compare three distinct model choices: (1) model 2 alone, that is, only Population II/I stars; (2) model 3, a bimodal model including the normal mode (model 2) plus the IM mode of Population III stars; and (3) model 1, a bimodal model including the normal model (model 2) plus the massive mode of Population III stars.

5.1 Reionization

Having set the SFR in our model, we now compute the electron scattering optical depth for our choice of the IMF. The evolution of the volume filling fraction of ionized regions is given by

$$\frac{\mathrm{d}Q_{\mathrm{ion}}(z)}{\mathrm{d}z} = \frac{1}{n_{\mathrm{b}}}\frac{\mathrm{d}n_{\mathrm{ion}}(z)}{\mathrm{d}z} - \alpha_{\mathrm{B}} n_{\mathrm{b}} C(z) Q_{\mathrm{ion}}^{2}(z)\,(1+z)^{3}\left|\frac{\mathrm{d}t}{\mathrm{d}z}\right|, \tag{9}$$

where n_{b} is the comoving density in baryons, $n_{\mathrm{ion}}(z)$ is the comoving density of ionizing photons, α_{B} is the recombination coefficient and $C(z)$ is the clumping factor. This factor is taken from Greif & Bromm (2006) and varies from a value of 2 at $z \leq 20$ to a constant value of 10 for $z < 6$. The escape fraction, f_{esc}, is set to 0.2 for both Population III and Population II/I. The number of ionizing photons for massive stars is calculated using the tables given in Schaerer (2002). Finally, the Thomson optical depth is computed as in Greif & Bromm (2006):

$$\tau = c\sigma_{\mathrm{T}} n_{\mathrm{b}} \int_{0}^{z} \mathrm{d}z'\, Q_{\mathrm{ion}}(z')(1+z')^{3}\left|\frac{\mathrm{d}t}{\mathrm{d}z'}\right|, \tag{10}$$

where z is the redshift of emission and σ_{T} is the Thomson scattering cross-section.

In Fig. 4, we plot the integrated optical depth from $z = 0$ to z. The red band represents the observed results from the *WMAP*7 (Komatsu et al. 2011). As one might expect, the normal mode alone (model 2 shown as the solid blue curve) is not capable of producing

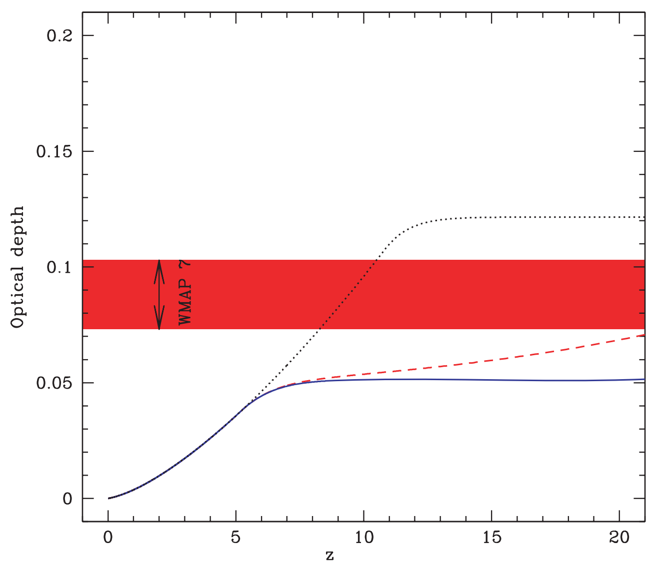

Figure 4. The optical depth as a function of the redshift. The red range corresponds to the observed results from the *WMAP*7 (Komatsu et al. 2011). The red dashed line corresponds to model 1 (with massive Population III stars), the blue solid line corresponds to model 2 (the normal mode) and the black dotted line corresponds to model 3 (with IM stars).

a sufficiently large optical depth. The massive mode (model 1 shown by the red dashed curve) does manage to reionize the IGM, but only barely. Of course, more reionization is possible by increasing the SFR for the massive mode, but this would lead to complications in elemental abundances. We see that the IM mode (model 3 – shown by the black dotted curve) is able to easily reionize the Universe compared to models 1 and 2. Our models allow an escape fraction as low as ∼0.1–0.2, which provides considerable flexibility in accounting for reionization. While the ratio of ionizing photons from a 6-$M_\odot$ star versus that from a 20-$M_\odot$ star is small, one has many additional stars in the IM scenario relative to the number in the massive mode.

5.2 Nucleosynthesis evolution

We next consider the evolution of the abundances of He, CNO, Fe and Mg as a function of the redshift and/or the metallicity. We also show the evolution of D and ^{7}Li due to early astration.

We begin with the evolution of the ^{4}He abundance. In the left-hand panel of Fig. 5, we show the analogue of Fig. 1 for the bimodal models based on the hierarchical structure formation. Plotted is the ^{4}He mass fraction, Y, versus [O/H]. The solid blue curve corresponds to the model with only a Population II/I contribution. This result is indistinguishable from that produced by models including the massive Population III contribution (not shown). This can be understood as the bulk of the ^{4}He and O are derived from the same stars in the two models. In both cases, the helium abundance begins at the BBN primordial value and remains rather flat until the oxygen abundance is roughy 1/10th of solar. In contrast, as shown by the black dotted curve, in the IM Population III model, ^{4}He is produced early in IM stars with little or no accompanied oxygen. As a result, the ^{4}He mass fraction begins to grow at very low [O/H] and for the model parameters chosen, plateaus at value close to $Y \approx 0.256$, in good agreement with recent determinations (Aver et al. 2010; Izotov & Thuan 2010). As in the case of the simple model discussed in Section 3, this model therefore produces an effective prompt initial enrichment of ^{4}He in low-metallicity galaxies. Note, however, that due to the size of the error bar associated with the observations, we cannot exclude the possibility that no enrichment occurred, leaving models 1 and 2 viable.

It is helpful to compare the helium–oxygen trend in Fig. 5(a) with the simple closed box results in Fig. 1. The latter shows results for different fractions $x_{\rm burst}$ of baryons processed through the IM mode. As noted above, our full hierarchical model cycles about 10 per cent of all baryons through IM stars; thus, Fig. 5(a) should be compared to the $x_{\rm burst} = 0.1$ curve in Fig. 1. Indeed, we see that both show very similar ^{4}He evolution.

In the right-hand panel of Fig. 5, we show the corresponding evolution of the ^{4}He abundance with the redshift. The dashed red curve corresponds to the massive Population III mode. Once again, the standard model and the massive Population III model show nearly identical histories. We do see, however, a modest increase in the helium mass fraction at high redshift due to the massive Population III mode. This is diluted by further infall as structures continue to grow. In the IM Population III model, there is a significant enhancement in the helium mass fraction around $z \sim 8$. This too is slightly diluted with the infall at later times.

We also show in Figs 6 and 7 the corresponding evolution for D and ^{7}Li; note that the vertical axes have zero offset in order to more clearly distinguish the model predictions. In each case, there is little difference between the standard model and the massive Population III model. IM stars, on the other hand, are known to deplete D/H (Fields et al. 2001). In this case, the degree of depletion is not severe (about 15 per cent), but it does move the BBN value farther away from the abundance determined in quasar absorption systems. The ^{7}Li astration factor is the same as for D/H and in this case moves the BBN value closer to the abundance determined in halo stars. However, an abundance of $\sim 4 \times 10^{-10}$ is still very far from the observed plateau value between $(1–2) \times 10^{-10}$.

Consider now the abundance evolution of CNOMg together with their abundance ratios. Figs 8 and 9 display the abundance evolution with z. As in all of the previous figures, each of the following figures shows three curves corresponding to a model with no Population III component (solid blue curve), a massive Population III component (red dashed curve) and a model with an IM Population III component (black dotted curve). The evolutionary behaviour of these model choices is well understood.

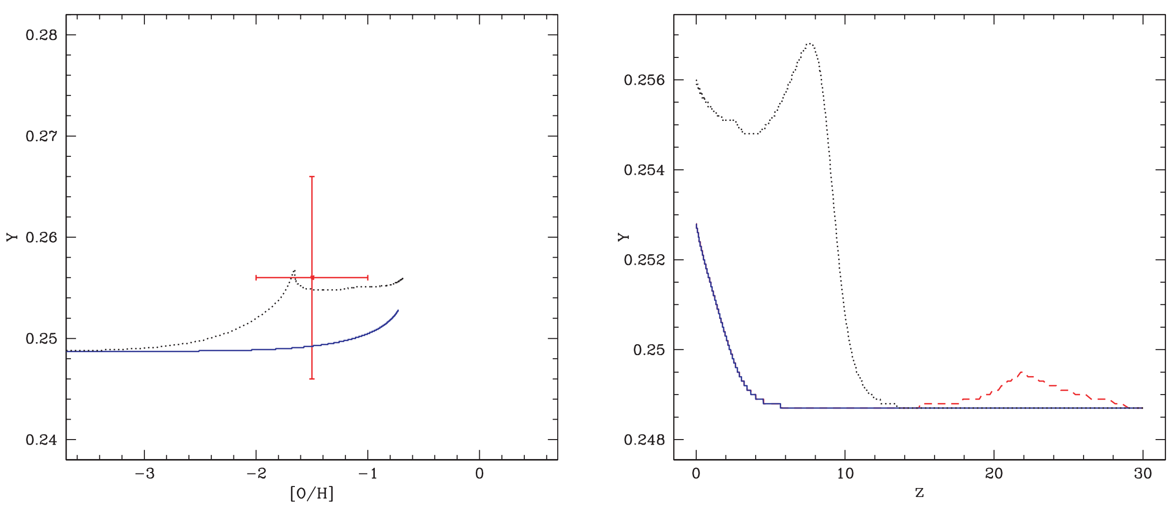

Figure 5. Left-hand panel: evolution of the helium mass fraction as a function of [O/H] (relative to the solar value). The solid blue line corresponds to models 2 (standard model) and 1 (with a massive Population III mode). The dotted black curve corresponds to model 3 (with IM Population III stars). The red point comes from Aver et al. (2010). Right-hand panel: evolution of the helium mass fraction as a function of the redshift. The red dashed line corresponds to the massive Population III model, the blue solid line corresponds to the standard model and the black dotted one corresponds to the IM Population III model.

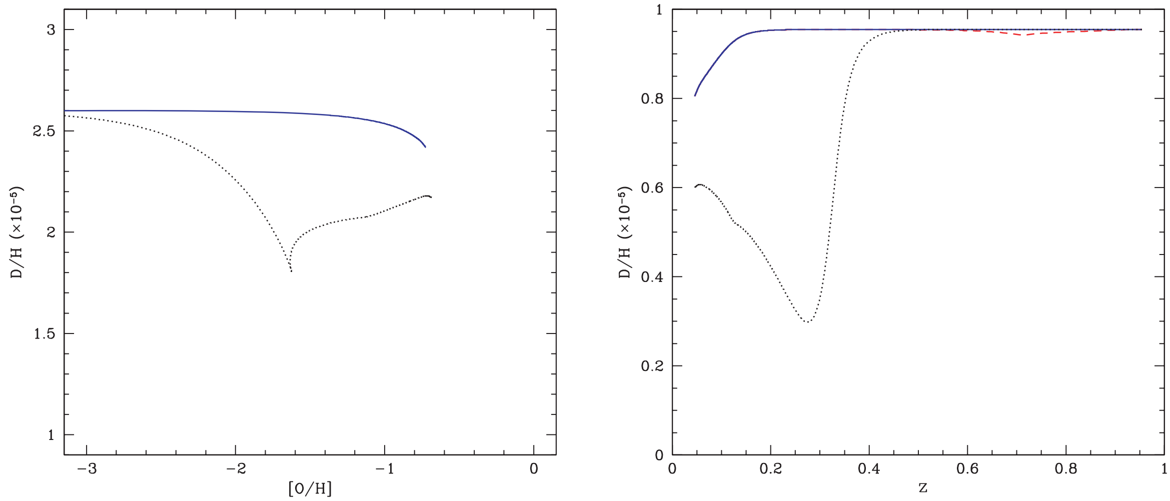

Figure 6. Left-hand panel: as in Fig. 5 showing the evolution of the deuterium abundance as a function of [O/H]. Right-hand panel: showing the evolution of the deuterium abundance with redshift. Note that the vertical axis is offset from zero, in order to more clearly show the (relatively small) effect on D.

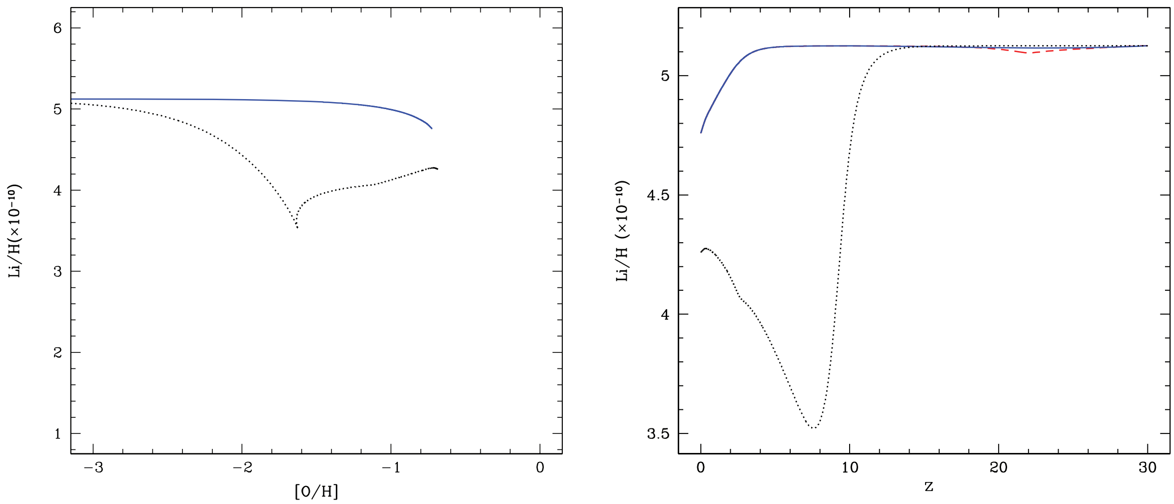

Figure 7. Left-hand panel: as in Fig. 5 showing the evolution of the lithium abundance as a function of [O/H]. Right-hand panel: showing the evolution of the lithium abundance with the redshift.

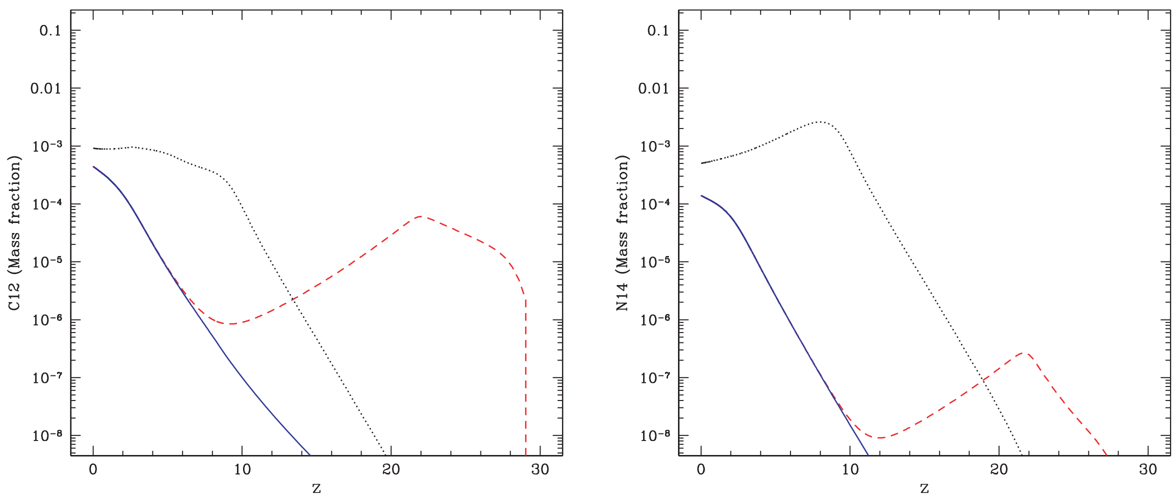

Figure 8. As in Fig. 5 for carbon (left-hand panel) and nitrogen (right-hand panel).

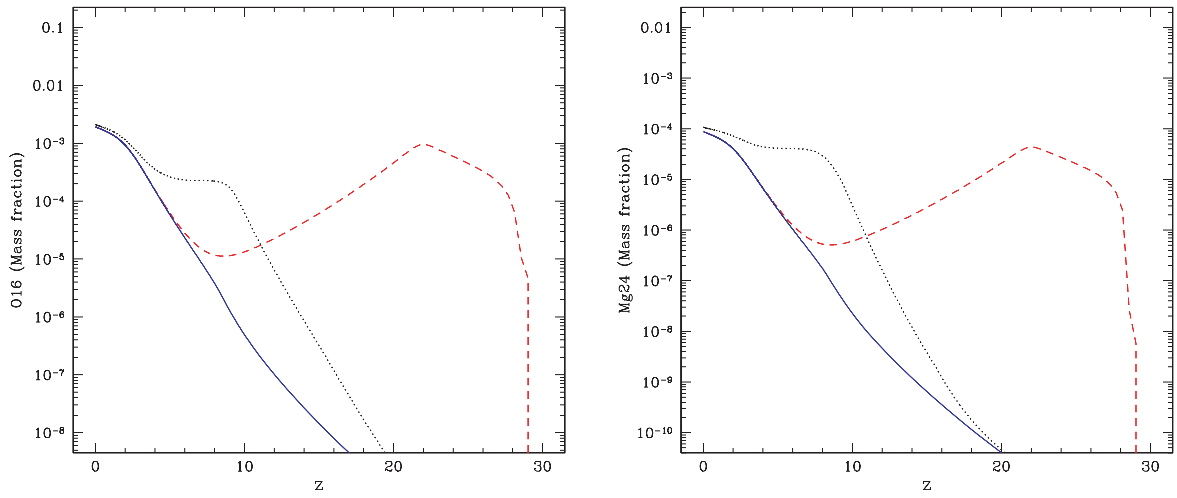

Figure 9. As in Fig. 5 for oxygen (left-hand panel) and magnesium (right-hand panel).

Normal mode stars produce a moderate abundance of heavy elements at high redshift from the IMF-suppressed massive stars in that mode. The same stars, nevertheless, are effective at low redshift and produce the bulk of metals observed in the Milky Way. The massive Population III component produces C, O and Mg at high redshift, though these abundances are diluted at low redshift by the infall as structures continue to grow. The IM stellar component produces a rather specific nucleosynthetic signature: essentially C and N.

Figs 10 and 11 show the evolution of the abundance ratios as a function of redshift. As one might expect, at lower redshifts, the IM-star Population III component produces the highest [O/Fe], [C/Fe] and [N/Fe]. The evolution of [Mg/Fe] corresponds to ^{24}Mg coming from massive stars and the highest value comes from the massive Population III component. The ratio of the neutron-rich isotopes to ^{24}Mg remains small in the Population III model dominated by massive stars, but this ratio can become large [$\mathcal{O}(1)$] in the IM Population III model. Also shown in these figures are the abundance ratios seen in several CEMPSs.

Surprisingly, the [C/O] ratio shown in Fig. 12 is high in this model as oxygen is also primarily produced in more massive stars whose role is diminished in this model at intermediate redshifts. In contrast, the massive Population III component reaches very high ratios of [C/Fe] and [O/Fe]. Only the massive Population III model is capable of reproducing the [O/Fe] abundance ratios observed in these stars. Similarly, the IM model has difficulty in achieving [C/Fe] ratios as high as the two HE stars with [C/Fe] ≈ 4 as seen in the figure, although the model does a reasonable job of accounting for the [C/O] ratios seen in these stars. The abundance patterns found in these CEMPSs continue to confirm that the formation of massive stars at very high redshift is plausible.

Finally, we consider the evolution of the parameter D_{trans} defined above in equation (4). Fig. 13 shows the D_{trans} parameter as a function of the metal enrichment. The black circles come from a compilation of Frebel et al. (2007). We see that this representation allows one to clearly distinguish the effects of the different choices of stellar mass ranges: the normal mode fits the bulk of standard stellar data. The massive mode can explain the few

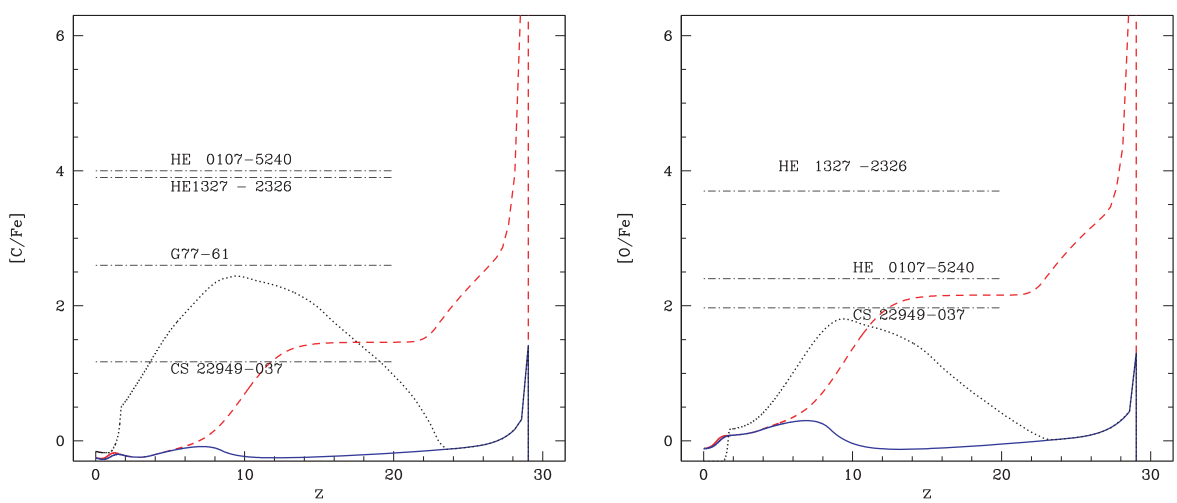

Figure 10. Left-hand panel: as in Fig. 5, the evolution of the [C/Fe] ratio (relative to the solar value) as a function of redshift. Right-hand panel: the evolution of the [O/Fe] ratio (relative to the solar value) as a function of redshift. Observational data (horizontal dashed lines) represent measured abundances in the following very iron poor halo stars: CS 22949−037 (Depagne et al. 2002), HE 0107−2240 (Bessel, Christlib & Gustafsson 2004), HE 1327−2326 (Frebel et al. 2005) and G77−61 (Plez & Cohen 2005).

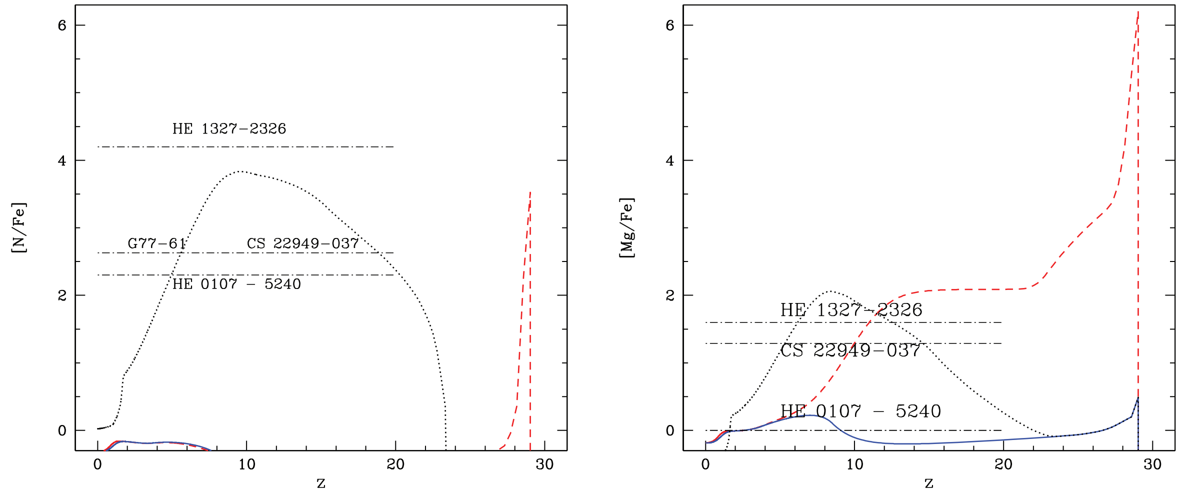

Figure 11. As in Fig. 10 for the [N/Fe] and [Mg/Fe] ratios.

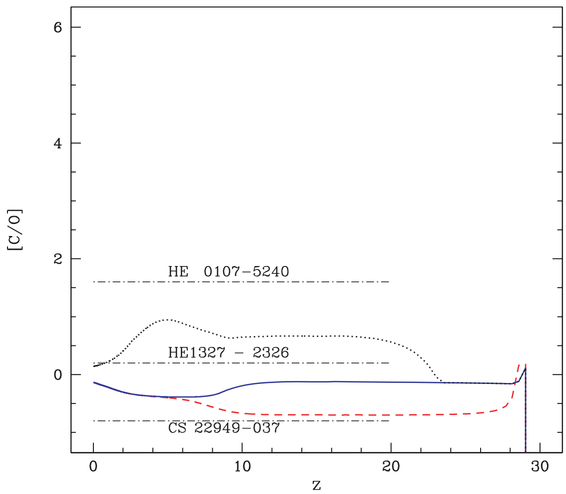

Figure 12. As in Fig. 10 for the [C/O] ratio.

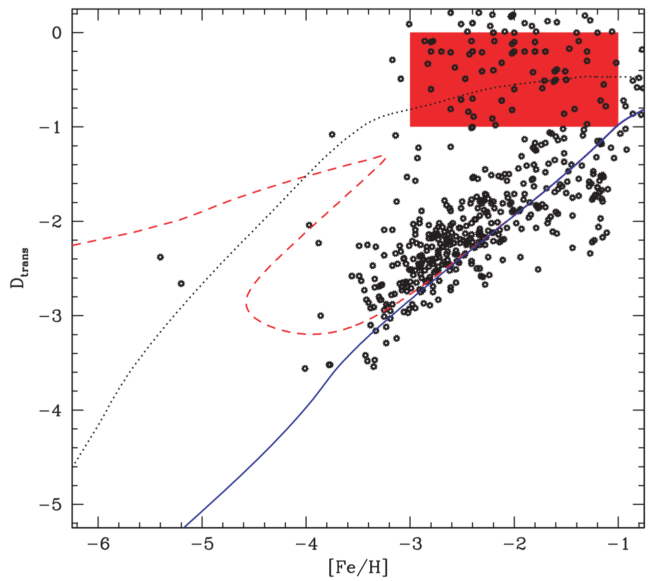

Figure 13. As in Fig. 5, the evolution of the $D_{\rm trans}$ parameter (transition discriminant $D_{\rm trans}$ – see equation 4) as a function of [Fe/H]. The black circles come from the compilation of Frebel et al. (2007). The red box corresponds to the region corresponding to C-rich stars.

CRUMPSs (Rollinde et al. 2009) and the IM stellar mode can explain the bulk of stars very enriched in C between $-3 <$ [Fe/H] $<$ -1 (red box). Indeed, we can see that the black dotted line (IM stars) is always much higher than the blue one (normal mode).

In particular, for [Fe/H] > -3, IM stars give $D_{\rm trans} \gtrsim -1$. In fig. 1 of Frebel et al. (2007), a specific stellar population is found exactly there: C-rich stars. It is very interesting to note that only the IM component is able to explain this part of the diagram. Indeed, to the best of our knowledge, the yield patterns of IM stars are the only ones which can correctly fit the abundances seen in C stars. Thus, it is tempting to interpret the metal-poor, C-rich stellar population as an indication of the presence of an early IM population. One could even push this further: of the stars in Fig. 13, about ∼10–20 per cent fall in the C-rich red box fitted by IM stars. To the extent that the data in the figure faithfully trace the ensemble of star-forming histories in the early universe, we would then estimate that Population III IM stars form at ∼10–20 per cent of our model rate. Since our IM model has ∼10 per cent of baryons processed through this mode, the C-rich stars would in turn imply that ∼1–2 per cent of baryons participate in the IM star formation.

Thus, we see that C-rich halo stars seem to demand *some* early IM star formation. Moreover, the large *scatter* in C and O abundance patterns over the full metal-poor halo star population demand that no single nucleosynthesis (and thus star-forming) history will suffice. Indeed, given that C-rich stars are outliers to the main trend, the IM population appears to be probably subdominant, acting only in low-mass galactic structures at high z.

5.3 Type II SNe

In Fig. 14, at high redshift, we show the resulting evolution of the SN II rate along with the data at relatively low redshift. The GOODS data for core-collapse SNe have been placed in two bins at $z = 0.4 \pm 0.2$ and 0.7 ± 0.2 (Dalhen et al. 2004, 2008). Their results (which have been corrected for the effects of extinction) show SN II rates which are significantly higher than the local rate (at $z = 0$; Cappelaro, Evans & Turatto 1999; Li et al. 2010). Since the timescale between the star formation and the core-collapse explosion is very short, there will be no significant contribution of Population

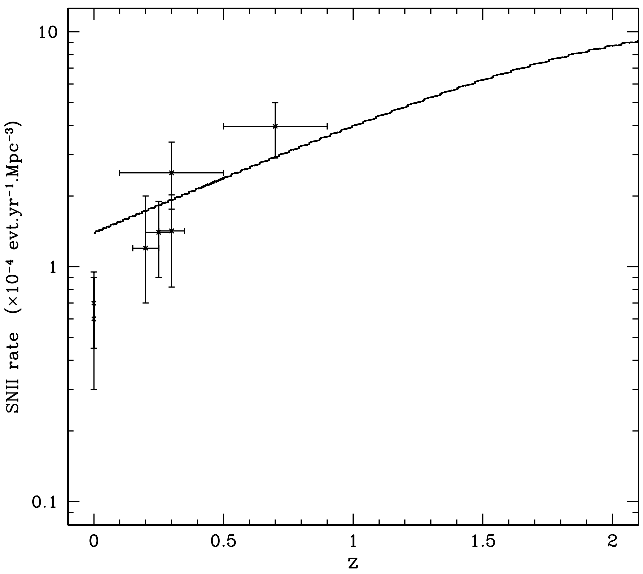

Figure 14. Evolution of the SNII rate as a function of the redshift. The observed rates are taken from Cappelaro et al. (1999), Capellaro et al. (2005), Dalhen et al. (2004, 2008), Botticella et al. (2008), Bazin et al. (2009) and Li et al. (2010). The evolution is the same for all three models.

III stars to SN II rates at any z. The SN II rate is directly related to the overall SFR and therefore to the astration rate ν and the slope of the SFR at high redshift.

The data at low z are well described by the models. This result is independent of our choice of the mass range for Population III, since massive Population III stars will only contribute to the SN rate at very high redshift and our IM Population III stars produce no SNe II. However, the model predicts much higher SN rates at higher redshift. Indeed, the SN II rate peaks at a redshift $z \approx 3$ at a rate which is nearly eight times the observed rate at low z. It will be interesting to see whether future data will be able to probe the SN rate at higher redshift. These elevated rates may be detectable in spite of the expected increase in dust extinction due to the early production of metals.

5.4 SNe Ia

Our calculation of the SN Ia rate depends on two additional assumptions beyond the specification of the models present in the previous section. The SN Ia rate will depend on the fraction of low-mass and IM stars which end up as SNe Ia, as well as the time-delay between the formation and explosion. Furthermore, it is not clear whether either of these quantities is a universal constant, that is, they may vary with the redshift, metallicity or the size of the structure the stars are formed in. We have assumed that the SN Ia rate is proportional to the IM-star formation rate (2–8 $M_{\odot}$). The coefficients adopted are $\epsilon = 0.02$ for the models 2, 1 and 0.01 for the model 3.

In Fig. 15, we show the SN Ia rate contrasted with the observational data. As in the case for SNe II, at high redshift, the data (also taken from the GOODS; Dalhen et al. 2004, 2008) are binned into four redshift bins at $z = 0.4$, 0.8, 1.2 and 1.6, each with a spread of ± 0.2. Other data references are given in the caption. We see that, in contrast to the case of SNe II, the evolution of the SN I rate is very different for the two models with and without IM stars. Adding the IM stellar mode implies a high SN Ia rate at high redshift. The position of this bump depends on the time-delay of the SN Ia.

Due to large uncertainties concerning the time-delay, we present two cases (Maoz, Sharon & Gal-Yam 2010; Totani et al. 2010). We hold the delay fixed at 2.5 Gyr for normal-mode stars, but in the left-hand panel of Fig. 15, we choose a delay of 3.4 Gyr and in the right-hand panel, we take 0.5 Gyr for model 3. While the normal mode fits the data quite well, we see that the population of IM stars creates a significant bump in the SN Ia rate at high redshift. Unless the time-delay for these SNe is reduced from the nominal value of 2.5 Gyr (as in the right-hand panel of Fig. 15), the SN Ia rate would greatly exceed the observed rate at redshifts between 1–1.5. If the delay is smaller, the bump in the SN Ia rate is pushed to higher redshift. Of course, it may be that for Population III stars, the fraction ϵ of IM stars becoming SNe Ia is reduced as discussed in Section 2.7.

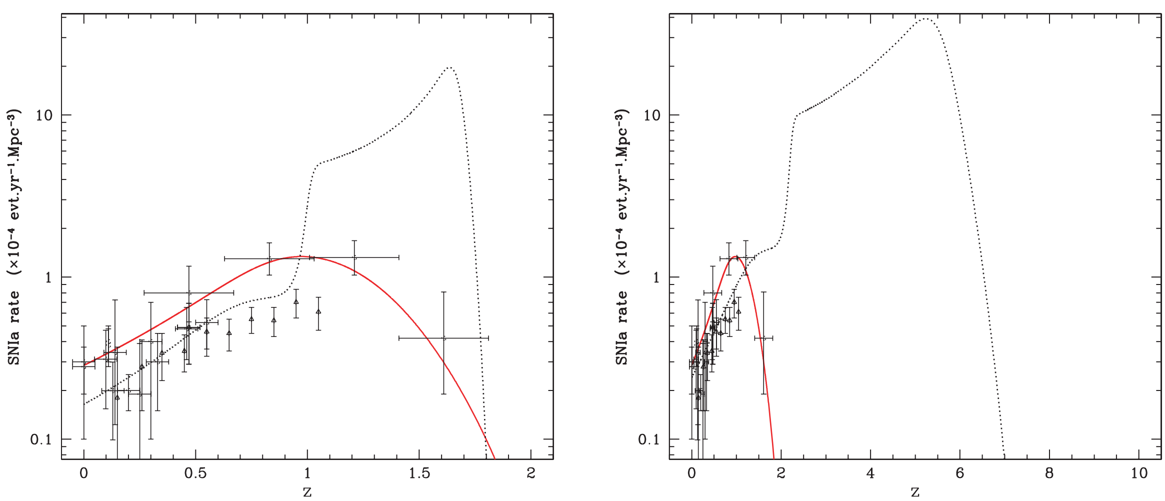

Figure 15. Evolution of the SN I rate as a function of the redshift. The observed rates are taken from Cappelaro et al. (1999), Reiss (2000), Hardin et al. (2000), Dalhen et al. (2004), Pain et al. (2002), Madgwick et al. (2003), Tonry et al. (2003), Strolger et al. (2004), Blanc et al. (2004), Li et al. (2010) and Perrett et al. (2010). The red solid curve corresponds to both models 1 (normal mode) and 2 (with massive Population III stars). The black dotted curve corresponds to model 3 (with IM stars). Left-hand panel: the assumed time-delays for IM stars in models 2 and 3 are 2.5 and 3.4 Gyr (including the lifetime of stars), respectively, and the fraction of the white dwarfs which become SNe Ia are $\epsilon = 2$ and 1 per cent, respectively. Right-hand panel: the time-delay for IM stars to become SNe Ia in model 3 is reduced to 0.5 Gyr and ϵ is 2 per cent for both models.

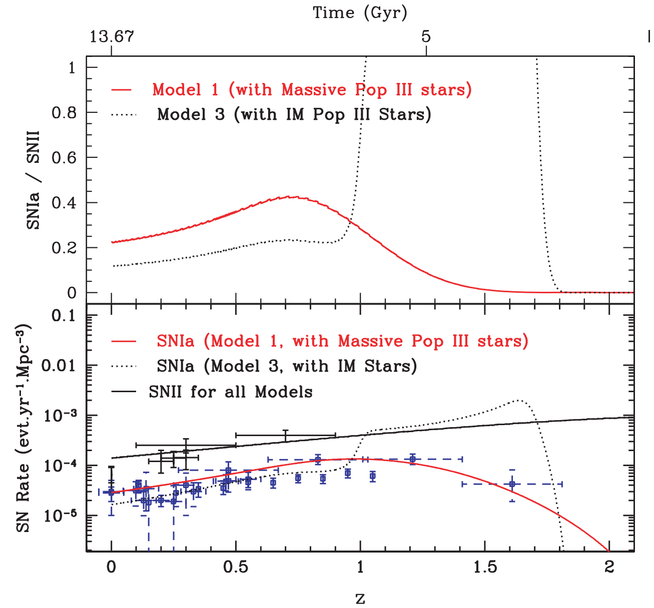

Figure 16. Evolution of the ratio of SN Ia and SN II event rates as a function of redshift. Top panel: for model 1 and model 3. In the bottom panel, the rates plotted of SNe I and SNe II as presented in Figs 14 and 15. The delay of SNe Ia is taken as 3.4 Gyr.

In the upper panel Fig. 16, the SN I/SN II ratio is plotted as a function of the redshift for models 1 and 3. In the lower panel of the figure, both SN Ia and SN II rates are plotted, as in Figs 14 and 15. The IM stellar mode predicts that the bulk of SNe Ia occur at hight redshift, though this result depends on the time-delay of these SNe. However, at such a high redshift, the selection efficiently drops rapidly towards zero (Perrett et al. 2010) and we cannot exclude the existence of this SN Ia component. In the future, it would be interesting to have an observational insight into low-mass galaxies, which could contain subluminous SNe Ia. As an alternative, if these subluminous SNe Ia are not observed, then we could put strong constraints on the early helium abundance in the primitive structures.

It is interesting to note the interplay between the IM constraints from halo star carbon abundances and from SNe Ia. Namely, at the end of Section 5.2, we argued that the existence of C-rich metal-poor halo stars seems to *require* an early cosmic IM star population, but the relative rarity of such C-rich stars also seems to imply that the IM population was subdominant, perhaps accounting for ~10–20 per cent of early star formation. Note that if we apply this same ~10–20 per cent factor to the IM predictions for SNe Ia in Figs 15 and 16, the predictions would be brought into agreement with the observations. Similarly, we could argue in the other direction, demanding that the IM fraction be small enough to agree with the SN Ia observations; this would again give ~10–20 per cent of our all-IM Population III model and thus would agree with the rough statistics suggested by the counts of C-rich metal poor stars. This rough concordance may be coincidental but is none the less both encouraging and intriguing.

6 DISCUSSION

By definition, as the first stars formed in a metal-free environment, Population III stars existed and played a role in our past history. However, the identity and mass distribution of these stars are largely unknown. We expect that they played an important role in reionizing the Universe at high redshift, as well as laid the chemical seeds for future generations of stars (Population II/I). We also know that a Salpeter IMF, typical of Population I with a mass range of 0.1–100 $M_\odot$, is not capable of producing a sufficient optical depth for the reionization or of producing the specific abundance patterns in EMPSs. Very massive stars (>100 $M_\odot$) also fail in producing the observed abundance patterns, though they are certainly capable of reionizing the Universe. A top-heavy IMF for Population III was studied in the cosmological context in Daigne et al. (2006) and Rollinde et al. (2009), and while successful in many aspects, this IMF is not capable of producing the (albeit weak) evidence for an enhancement in ^{4}He at low metallicity over BBN predictions or the large carbon enhancements which are made to manifest in the parameter D_{trans}. To the best of our knowledge, IM stars as candidates for Population III have not been studied in the cosmological context up to now.

We have shown that an early generation of IM stars is indeed capable of providing an effective prompt initial enrichment of He. We have also shown, perhaps surprisingly, that these stars normalized in abundance to the required He enrichment are more than capable of providing a sufficient number of ionizing photons to the early IGM. Also as a bonus, IM stars can provide large abundance ratios of C, N, O and Mg relative to Fe in EMPSs. However, our results indicate that one cannot simply assume a homogeneous and well-mixed IGM and/or ISM as smaller structures grow to large galaxies and clusters of galaxies. The CNO abundance that this model predicts at metallicities between $-3 < [Fe/H] < -1$ far surpasses the abundances observed in the IGM.

We are thus led to an interesting dilemma which is best characterized by the data displayed in Fig. 13. Recall that the discriminant D_{trans} represents a measure of carbon and oxygen produced in prior generations of stars. As discussed earlier, the data show two distinct populations: the bulk of the data show increasing D_{trans} with [Fe/H] and is very well modelled by either a standard or a top-heavy IMF, and a second population with very large D_{trans} between $-3 <$ [Fe/H] < -1. The latter is well explained by our Population III IM stellar mode. How can one model explain both populations?

It is perhaps too naive to expect a homogeneous model as the type we have been describing to explain this discrepancy. Indeed one can imagine that the impact of the generation of IM stars was effective only early on in the building of higher mass objects in the hierarchical structure formation scenario, that is, this generation was active only in the smallest-scale structures, here taken to be typically 10^7 $M_\odot$. These structures and the low-mass stars and remnants left behind were in some cases incorporated into the haloes of larger objects to become galaxies. Others remain as low-mass dwarfs. In this way, one can perhaps explain the bulk of the observations of low and increasing D_{trans} in stars formed in larger scale objects involving a larger baryon fraction, while those stars with large D_{trans} would be explained by the impact of IM stars in the smallest structures formed. Indeed, using both carbon data on metal-poor stars and SN Ia observations, we roughly estimate that a Population III IM mode operates at ~10–20 per cent of our model rate. Since our IM mode processes about 10 per cent of baryons, this in turn implies that ~1–2 per cent of baryons participate in the IM star formation.

In this interpretation, the prompt initial enrichment of ^{4}He, which is observed largely in dwarf irregular galaxies, was also impacted by IM stars as these objects were evidently not incorporated into larger scale structures. In the context of the light-element abundances, it is interesting to note further that some of the stars which show large carbon enhancements also show deficiencies in ^{7}Li. Furthermore, there is increasing evidence (Meléndez et al. 2010; Sbordone et al.

2010) for a breakdown of the Spite plateau at metallicities below [Fe/H] < -3. In Sbordone et al. (2010), it is argued that the depletion (which shows considerable dispersion *below* the plateau) at low metallicity may have been due to the stellar astration. The model discussed here (given the above interpretation) can account for most of the astration seen in these stars. The model cannot, however, account for the discrepancy between the BBN prediction at the *WMAP* baryon density and the Spite plateau value as speculated in Piau et al. (2006). Note that the depletion in D/H is probably not an issue, as the absorption systems with measured D/H are presumably larger scale structures for which our abundance patterns would not be expected to apply.

Unfortunately, neither of the two Population III models delivers entirely satisfactory results. While the massive mode is capable of producing sufficiently high ratios of [C, O, Mg/Fe] to explain the observations of extremely iron-poor stars, the high ratios occur almost instantly after the first stars are born and thus require these stars to be born at that time at very high redshift. This model also has difficulty in explaining the high [N/Fe] or [C/O] ratios seen. As a result, the massive Population III model cannot explain the high values of $D_{\rm trans}$ seen in some stars. The model cannot account for the effective prompt initial enrichment of ^{4}He nor can it be used to account for the astration of ^{7}Li below the Spite plateau. On the other hand, the IM model for Population III underproduces [O/Fe] and because of the large amounts of C and N produced cannot explain the bulk of the values of $D_{\rm trans}$ observed, but the top panel data are explained due to the overabundances of C and N. Indeed, the overproduction of these elements would preclude the homogeneous and well-mixed treatment of gas in ever-increasing large-scale structures.

Another distinctive feature of the IM Population III model is the prediction for the rate of SNe Ia at high redshift. This model naturally predicts a large increase in the SN Ia rate *if* the efficiency for SNe is constant and the time-delay is not small. It is relevant to speculate that a small high-mass tail in the IM population could lead to possible gamma-ray bursts (GRBs) in the redshift range 10–20. This would fill the 'GRB desert' between the Population II and usual high-redshift Population III stars.

ACKNOWLEDGMENTS

The work of KAO was supported in part by DOE grant DE–FG02–94ER–40823 at the University of Minnesota plus PICS CNRS/USA. We are indebted to F. Daigne for his permanent help. Thanks very much to Anna Frebel for the use of her data table compilation. Thanks also to Yannick Mellier and Reynald Pain for their precious help regarding the SNIa rate observations. Finally, we warmly thank the referee for her(his) very useful comments and suggestions.

REFERENCES

Abia C., Domínguez I., Straniero O., Limongi M., Chieffi A., Isern J., 2001, ApJ, 557, 126
Alcock C. et al., 2000, ApJ, 542, 281
Alibés A., Labay J., Canal R., 2001, A&A, 370, 1103
Aoki W. et al., 2001, ApJ, 561, 346
Aoki W., Norris J. E., Ryan S. G., Beers T. C., Ando H., 2002, ApJ, 567, 1166
Ashenfelter T. P., Mathews G. J., Olive K. A., 2004, ApJ, 615, 82
Asplund M., Lambert D. L., Nissen P. E., Primas F., Smith V. V., 2006, ApJ, 644, 229
Aver E., Olive K. A., Skillman E. D., 2010, J. Cosmol. Astropart. Phys., 05, 003
Bazin G. et al., 2009, A&A, 499, 653
Bennett D. P., 2005, ApJ, 633, 906
Bessel M. S., Christlib N., Gustafsson B., 2004, ApJ, 612, L61
Blanc G. et al., 2004, A&A, 423, 881
Bonifacio P. et al., 2007, A&A, 462, 851
Boothroyd A. I., Sackmann I.-J., Wasserburg G. J., 1995, ApJ, 442, L21
Botticella M., T. et al., 2008, A&A, 479, 49
Bouwens, R. J. et al., 2010, ApJ, 709, L133
Briley M. M., Harbeck D., Smith G. H., Grebel E. K., 2004, AJ, 127, 1588
Bromm V., 2004, PASP, 116, 103
Bromm V., Larson R. B., 2004, ARA&A, 42, 79
Bromm V., Loeb A., 2003, Nat, 425, 812
Bromm V., Yoshida N., Hernquist L., McKee C. F., 2009, Nat, 459, 49
Cappellaro E., Evans R., Turatto, 1999, A&A, 351, 459
Cappellaro E. et al., 2005, A&A, 430, 83
Cen R., 2003, ApJ, 591, L5
Chabrier G., 2004, ApJ, 611, 315
Ciardi B., Ferrara A., 2005, Space Sci. Rev., 116, 625
Coc A., Vangioni E., 2010, J. Phys. Conf. Ser., 202, 012001
Coc A., Vangioni-Flam E., Cassé M., Rabiet M., 2002, Phys. Rev. D, 65, 043510
Coc A., Vangioni-Flam E., Descouvemont P., Adahchour A., Angulo C., 2004, ApJ, 600, 544
Cooke, R., Pettini M., Steidel C. C., Rudie G. C., Jorgenson R. A., 2010, MNRAS, doi:10.1111/j.1365-2966.2010.17966.x
Cuoco A., Iocco F., Mangano G., Miele G., Pisanti O., Serpico P. D., 2004, Int. J. Mod. Phys. A, 19, 4431
Cyburt R. H., 2004, Phys. Rev. D, 70, 023505
Cyburt R. H., Fields B. D., Olive K. A., 2001, New Astron., 6, 215
Cyburt R. H., Fields B. D., Olive K. A., 2002, Astropart. Phys., 17, 87
Cyburt R. H., Fields B. D., Olive K. A., 2003, Phys. Lett. B, 567, 227
Cyburt R. H., Fields B. D., Olive K. A., 2008, J. Cosmol. Astropart. Phys., 11, 12
Dahlen T. et al., 2004, ApJ, 613, 189
Dahlen T., Strolger L. G., Riess A., 2008, ApJ, 681, 469
Daigne F., Olive K. A., Vangioni-Flam E., Silk J., Audouze J., 2004, ApJ, 617, 693
Daigne F., Olive K. A., Silk J., Stoehr F., Vangioni E., 2006, ApJ, 647, 773
Davé R., 2008, MNRAS, 385, 147
Depagne E. et al., 2002, A&A, 390, 187
Descouvemont P., Adahchour A., Angulo C., Coc A., Vangioni-Flam E., 2004, At. Data Nucl. Data Tables, 88, 203
Ekström S., Meynet G., Chiappini C. Hirschi R., Maeder A., 2008, A&A, 489, 685
Fenner Y., Gibson B. K., Lee H.-c., Karakas A. I., Lattanzio J. C., Chieffi A., Limongi M., Yong D., 2003, PASA, 20, 340
Fields B. D., Olive K. A., Silk J., Cassé M., Vangioni-Flam E., 2001, ApJ, 563, 653
Frebel A., 2010, Astron. Nachrichten, 331, 474
Frebel A., Bromm V., 2010, MNRAS, submitted (arXiv:1010.1261)
Frebel A. et al., 2005, Nat, 434, 871
Frebel A., Johnson J. L., Bromm V., 2007, MNRAS, 380, L40
Fujimoto M. Y., Ikeda Y., Iben I., Jr, 2000, ApJ, 529, L25
Gonzalez V., Labbé I., Bouwens R., Illingworth G., Fraux N., Kriek N., Brammer G., 2010a, ApJ, 713, 115
Gonzalez V., Labbé I., Bouwens R., Illingworth G., Fraux N., Kriek N., 2010b, preprint (arXiv:1008.3901)
Greif T. H., Bromm V., 2006, MNRAS, 373, 128
Haiman Z., Holder G. P., 2003, ApJ, 595, 1
Harbeck D., Smith G. H., Grebel E. K., 2003, AJ, 125, 197
Hardin D. et al., 2000, A&A, 362, 419
Hopkins A. M., Beacom J. F., 2006, ApJ, 651, 142
Hosford A., Ryan S. G., García Pérez A. E., Norris J. E., Olive K. A., 2009, A&A, 493, 601
Hosford A., García Pérez A. E., Collet R., Ryan S. G., Norris J. E., Olive K. A., 2010, A&A, 511, 47
Hoversten E. A., Glazebrook K., 2008, ApJ, 675, 163

Hultman Kramer R. H., Haiman Z., Madau P., 2010, preprint (arXiv:1007.3581)
Izotov Y. I., Thuan T. X., 2010, ApJ, 710, L67
Izotov Y. I., Thuan T. X., Lipovetsky V. A., 1994, ApJ, 435, 647
Izotov Y. I., Thuan T. X., Stasinska G., 2007, ApJ, 662, 15
Johnson J., Greif T., Bromm V., Klessen R., Ippolito J., 2009, MNRAS, 399, 37
Karakas A. I., Lattanzio J. C., 2003, PASA, 20, 279
Karakas A., Lattanzio J., 2007, PASA, 24, 103
Karlsson T., Johnson J., Bromm V., 2008, ApJ, 679, 6
Kogut A. et al., 2003, ApJS, 148, 161
Komatsu E. et al., 2009, ApJS, 180, 330
Komatsu E., et al., 2011, ApJS, 192, 18
Labbe I., Gonzalez V., Bouwens R. J., 2010, ApJ, 716, L103
Li W. et al., 2010, preprint (arXiv:1006.4613)
Lucatello S., Tsangarides S., Beers T. C., Carretta E., Gratton R. G., Ryan S. G., 2005, ApJ, 625, 825
Madgwick D. S. et al., 2003, ApJ, 599, L33
Maeder A., Meynet G., 1989, A&A, 210, 155
Maoz D., Sharon K., Gal-Yam A., 2010, ApJ, 722, 1879
Mattsson L., 2010, A&A, 515, 68
Meléndez J., Casagrande L., Ramírez I., Asplund M., Schuster W. J., 2010, A&A, 515, L3
Meurer G. R. et al., 2009, ApJ, 695, 765
Nomoto K., Uenishi T., Kobayashi C., Umeda H., Ohkubo T., Hachisu I., Kato M., 2003, in Hillebrandt W., Leibundgut B., eds, From Twilight to Highlight: The Physics of Supernovae. Springer-Verlag, Berlin, p. 115
Olive K. A., Skillman E. D., 2001, New Astron., 6, 119
Olive K. A., Skillman E. D., 2004, ApJ, 617, 29
Pain R. et al., 2002, ApJ, 577, 120
Peimbert M., Peimbert A., Ruiz M. T., 2000, ApJ, 541, 688
Peimbert M., Luridiana V., Peimbert A., 2007, ApJ, 666, 636
Perrett K. et al., 2010, AJ, 140, 518
Pettini M., Zych B. J., Murphy M. T., Lewis A., Steidel C. C., 2008, MNRAS, 391, 1499
Piau L., Beers T. C., Balsara D. S., Sivarani T., Truran J. W., Ferguson J. W., 2006, ApJ, 653, 300
Plez B., Cohen J. G., 2005, A&A, 434, 1117
Porter R. L., Ferland G. J., MacAdam K. B., 2007, ApJ, 657, 327
Press W. H., Schechter P., 1974, ApJ, 187, 425
Reiss D., 2000, PhD thesis, Univ. Washington
Robertson, B. E., Ellis R., Dunlop J., McLure J., Stark D., 2010, Nat, 468, 55
Rollinde E., Vangioni E., Maurin D., Olive K. A., Daigne F., Silk J., Vincent F. H., 2009, MNRAS, 398, 1782
Rossi S., Beers T. C., Sneden C., 1999, in Gibson B. K., Axelrod T. S., Putman M. E., eds, ASP Conf. Ser. Vol. 165, Carbon Abundances for Metal-Poor Stars Based on Medium-Resolution Spectra. Astron. Soc. Pac., San Francisco, p. 264
Ryan S. G., Beers T. C., Olive K. A., Fields B. D., Norris J. E., 2000, ApJ, 530, L57
Safranek-Shrader C., Bromm V., Milosavljević M., 2010, ApJ, 723, 1568
Sbordone L. et al., 2010, A&A, 522, 26
Schaerer D., 2002, A&A, 382, 28
Schneider R., Omukai K., 2010, MNRAS, 402, 429
Serpico P. D., Esposito S., Iocco F., Mangano G., Miele G., Pisanti O., 2004, J. Cosmol. Astropart. Phys., 12, 10
Shetrone M. D., 1996, AJ, 112, 2639
Sivarani T. et al., 2004, A&A, 413, 1073
Smith B. D., Turk M. J., Sigurdsson S., O'Shea B. W., Norman M. L., 2009, ApJ, 691, 441
Spite F., Spite M., 1982, A&A, 115, 357
Spite M., François P., Nissen P. E., Spite F., 1996, A&A, 307, 172
Springel V., Hernquist L., 2003, MNRAS, 339, 312
Stacy A., Bromm V., Loeb A., 2011, MNRAS, doi:10.1111/j.1365-2966.2010.18152.x
Strolger I. L. et al., 2004, ApJ, 613, 200
Sullivan M., Conley A., Howell D. A., Neill J. D., 2010, MNRAS, 406, 782
Tisserand P. et al., 2007, A&A, 469, 387
Tonry J. L. et al., 2003, ApJ, 594, 1
Torres S., Camacho J., Isern J., Garcia-Berro E., 2010, A&A, 511, 88
Totani T., Morokuma T., Odu T., Doi N., 2008, PASJ, 60, 1327
Umeda H., Nomoto K., 2005, ApJ, 619, 427
van den Hoek L. B., Groenewegen M. A. T., 1997, A&AS, 123, 305
van Dokkum P. G., 2008, ApJ, 674, 29
Venkatesan A., Schneider R., Ferrara A., 2004, MNRAS, 349, L43
Wilkins S. M., Hopkins A. M., Trentham N., Tojeiro R., 2008a, MNRAS, 391, 363
Wilkins S. M. N., Trentham N., Hopkins A. M., 2008b, MNRAS, 385, 687
Wise J. H., Cen R., 2009, ApJ, 693, 984
Woosley S. E., Weaver T. A., 1995, ApJS, 101, 181
Wyithe J. S. B., Loeb A., 2003, ApJ, 588, L69
Yong D., Lambert D. L., Ivans I. I., 2003a, ApJ, 599, 1357
Yong D., Grundahl F., Lambert D. L., Nissen P. E., Shetrone M. D., 2003b, A&A, 402, 985
Yoshii Y., Saio H., 1986, ApJ, 301, 587

This paper has been typeset from a TEX/LATEX file prepared by the author.